Physical Oceanographic Study at the Rockland Disposal Site
August 2001

Disposal Area Monitoring System DAMOS

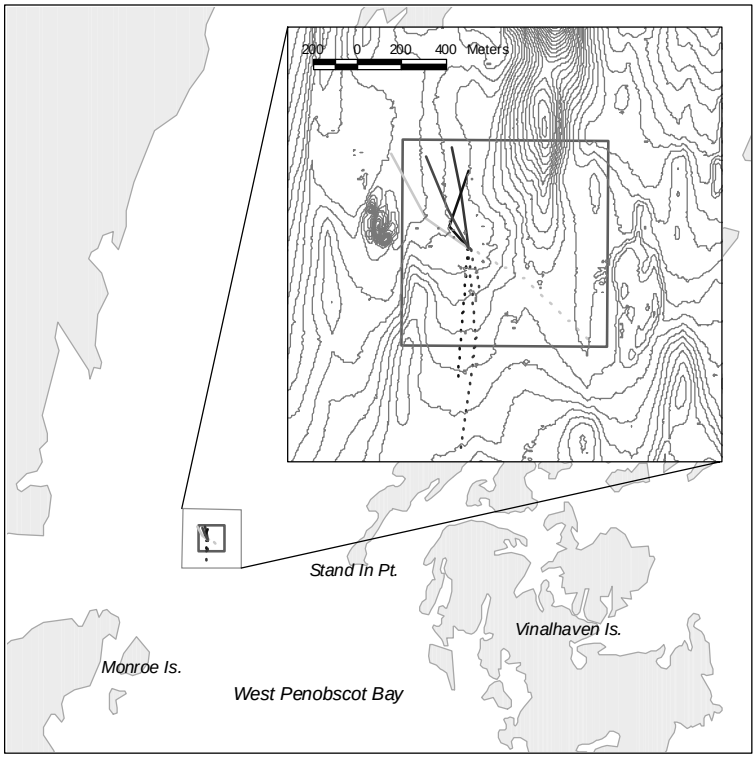

D A M O S

DISPOSAL AREA MONITORING SYSTEM

Contribution 145
March 2003

US Army Corps of Engineers ®
New England District

REPORT DOCUMENTATION PAGE

form approved
OMB No. 0704-0188

1. AGENCY USE ONLY (LEAVE BLANK)	2. REPORT DATE	3. REPORT TYPE AND DATES COVERED
	March 2003	FINAL REPORT

4. TITLE AND SUBTITLE
Physical Oceanographic Study at the Rockland Disposal Site, August 2001

5. FUNDING NUMBERS

6. AUTHOR(S)
Science Applications International Corporation

7. PERFORMING ORGANIZATION NAME(S) AND ADDRESS(ES)
Science Applications International Corporation
221 Third Street
Newport, RI 02840

8. PERFORMING ORGANIZATION REPORT NUMBER
SAIC No. 579

9. SPONSORING/MONITORING AGENCY NAME(S) AND ADDRESS(ES)
US Army Corps of Engineers-New England District
696Virginia Rd
Concord, MA 01742-2751

10. SPONSORING/MONITORING AGENCY REPORT NUMBER
Contribution No. 145

11. SUPPLEMENTARY NOTES
Available from DAMOS Program Manager, Regulatory Division
USACE-NAE, 696 Virginia Rd, Concord, MA 01742-2751

12a. DISTRIBUTION/AVAILABILITY STATEMENT
Approved for public release; distribution unlimited

12b. DISTRIBUTION CODE

13. ABSTRACT

The Disposal Area Monitoring System (DAMOS) Program sponsored a physical oceanographic study at the Rockland Disposal Site (RDS) located in West Penobscot Bay in August 2001. The disposal site has been subjected to limited dredged material deposition in recent decades; however, potential channel maintenance and coastal construction projects in the future could yield significant volumes of dredged material suitable for unconfined disposal at RDS. Thus, it was deemed prudent to update existing information related to oceanographic conditions and processes within the disposal site as a basis for numerical modeling routines that predict the fate of dredged material disposal plumes in the water column. A bottom-mounted instrument array consisting of an acoustic Doppler current profiler (ADCP), an acoustic Doppler current meter (ADCM), and an optical backscatter sensor (OBS) mounted on an aluminum frame was deployed near the center of the disposal site for a full month tidal cycle.

Data from the current meters showed that the semidiurnal lunar tidal signal dominates the currents throughout the water column. The time series records of currents showed that the mid-water column currents were strongest, and that the Spring-Neap tidal cycle was significant at all depths. Long term mean currents were weak (<3 cm·s^{-1}), and mean direction ranged from north to east from the surface to bottom, respectively. A harmonic tidal analysis confirmed the semidiurnal tide as most significant, but failed to delineate the fortnightly or monthly tide with confidence. Variance from the tidal analysis showed the currents to be nearly 95% tidal at many depth levels. Tidal ellipses showed the currents to be extremely rectilinear, with almost no minor axis at some depth levels. A record of residual currents, calculated by subtracting the least squares tidal fit from the raw current data, showed weak non-tidal currents, with the strongest events in the near surface. Data from the OBS sensor showed that significant turbidity events were rare at RDS, and were not associated with increases in tidal current velocity. As a result, increases in turbidity over RDS were attributed to the advection of turbid waters from outside the disposal site. An analysis of Total Suspended Solids (TSS) from water samples collected at the beginning and end of the deployment period showed that the bottom water had minimal amounts of suspended sediment.

14. SUBJECT TERMS Rockland Disposal Site, Dredged Material, Currents, Turbidity, Resuspension

15. NUMBER OF TEXT PAGES: 39

16. PRICE CODE

17. SECURITY CLASSIFICATION OF REPORT	18. SECURITY CLASSIFICATION OF THIS PAGE	19. SECURITY CLASSIFICATION OF ABSTRACT	20. LIMITATION OF ABSTRACT
Unclassified			

PHYSICAL OCEANOGRAPHIC STUDY AT THE ROCKLAND DISPOSAL SITE AUGUST 2001

CONTRIBUTION #145

March 2003

Report No.
SAIC-579

Submitted to:

Regulatory Division
New England District
U.S. Army Corps of Engineers
696 Virginia Road
Concord, MA 01742-2751

Submitted by:
Science Applications International Corporation
Admiral's Gate
221 Third Street
Newport, RI 02840
(401) 847-4210

US Army Corps
of Engineers ®
New England District

TABLE OF CONTENTS

Page

LIST OF TABLES

LIST OF FIGURES

Page

Page

EXECUTIVE SUMMARY

The Disposal Area Monitoring System (DAMOS) Program sponsored a physical oceanographic study at the Rockland Disposal Site (RDS) located in West Penobscot Bay in August 2001. The disposal site has been subjected to limited dredged material deposition in recent decades; however, potential channel maintenance and coastal construction projects in the future could yield significant volumes of dredged material suitable for unconfined disposal at RDS. Thus, it was deemed prudent to update existing information related to oceanographic conditions and processes within the disposal site as a basis for numerical modeling routines that predict the fate of dredged material disposal plumes in the water column.

Science Applications International Corporation (SAIC) deployed a bottom-mounted instrument array consisting of an acoustic Doppler current profiler (ADCP), an acoustic Doppler current meter (ADCM), and an optical backscatter sensor (OBS) mounted on an aluminum frame for a full month tidal cycle at a position of 44°07.093´ N, 69°00.388´ W. The ADCP provided data on the currents throughout the water column, and the ADCM provided data on the near-bottom currents and temperature, as well as water level. The OBS sensor, which was interfaced with the ADCM, provided data on the relative turbidity at the near-bottom level. A water sample was collected 75 cm above the seafloor upon deployment and recovery of the instrument array, and a hydrocast was performed with a conductivity-temperature-depth profiler (CTD) to examine suspended sediment load and physical characteristics of the water column.

Data from the current meters showed that the semidiurnal lunar tidal signal dominates the currents throughout the water column. The time series records of currents showed that the mid-water column currents were strongest, and that the Spring-Neap tidal cycle was significant at all depths. Long term mean currents were weak (< 3 cm·s^{-1}), and mean direction ranged from north to east from the surface to bottom, respectively. A harmonic tidal analysis confirmed the semidiurnal tide as most significant, but failed to delineate the fortnightly or monthly tide with confidence. Variance from the tidal analysis showed the currents to be nearly 95% tidal at many depth levels. Tidal ellipses showed the currents to be extremely rectilinear, with almost no minor axis at some depth levels. A record of residual currents, calculated by subtracting the least squares tidal fit from the raw current data, showed weak non-tidal currents, with the strongest events in the near surface. Trends in the near-surface residual currents mimicked the meteorological trends observed at a nearby buoy maintained by the University of Maine.

Data from the OBS sensor showed that significant turbidity events were rare at RDS, and were not associated with increases in tidal current velocity. As a result, increases in turbidity over RDS were attributed to the advection of turbid waters from outside the disposal site. An analysis of Total Suspended Solids (TSS) from water samples collected at the beginning and end of the deployment period showed that the bottom water had minimal amounts of suspended sediment.

1.0 INTRODUCTION

As part of the Disposal Area Monitoring System (DAMOS) sponsored by the US Army Corps of Engineers, New England District (NAE), Science Applications International Corporation (SAIC) conducted a physical oceanographic study within the confines of the Rockland Disposal Site (RDS) in Maine. This effort serves as a follow-on study to the last full-scale environmental monitoring survey conducted at RDS in September 2000 (SAIC 2001).

The Rockland Disposal Site is one of three regional dredged material disposal sites located in the waters of Maine. RDS covers a 0.865 km^2 (0.25 nmi^2) area of seafloor within West Penobscot Bay and is centered at 44°07.105´ N, 69°00.269´ W (NAD 83). It is located approximately 5.7 km (3.1 nmi) east-southeast of Brewster Point, Glen Cove, Maine (Figure 1-1). Sediments deposited at RDS have originated from dredging projects in Rockland, Camden, and Castine Harbors, as well as Bangor, Belfast, and Searsport. However, due the intermittent nature of disposal at RDS, monitoring efforts have not been as intensive as those at other sites in New England (e.g., Portland Disposal Site, Central Long Island Sound Disposal Site).

During the 1980s, RDS received an average annual dredged material disposal volume of nearly 110,000 m^3 (Morris 1996). These sediments were deposited at the US Coast Guard, Class-A, Special Purposes buoy designated "DG" and located near the center of the disposal site at 44°07.180´ N, 69°00.364´ W. However, the lack of major improvement and maintenance dredging in the Penobscot Bay region during the 1990s led to a drastic reduction in the volume of dredged material placed at RDS. Between April 1990 and May 2000, a total reported barge volume of 26,360 m^3 from multiple small projects was deposited in close proximity to the DG buoy (see disposal logs in Appendix A). A renewed interest has developed in maintaining the approaches into the many harbors that exist within the region. In addition, proposed infrastructure improvements at the head of the bay could yield significant volumes of material suitable for unconfined open water disposal at RDS.

In order to better understand and forecast the behavior of dredged material placed at RDS, near-bottom and water column current data were collected over a full 28-day tidal cycle. These data were collected to evaluate physical oceanographic conditions at the disposal site, as well as support dredged material disposal modeling efforts using the Short Term Fate (STFATE) and Multiple Dump Fate (MDFATE) disposal models. In support of this effort, SAIC deployed an instrument array consisting of two current meters and an optical backscatter sensor for a period of 32 days.

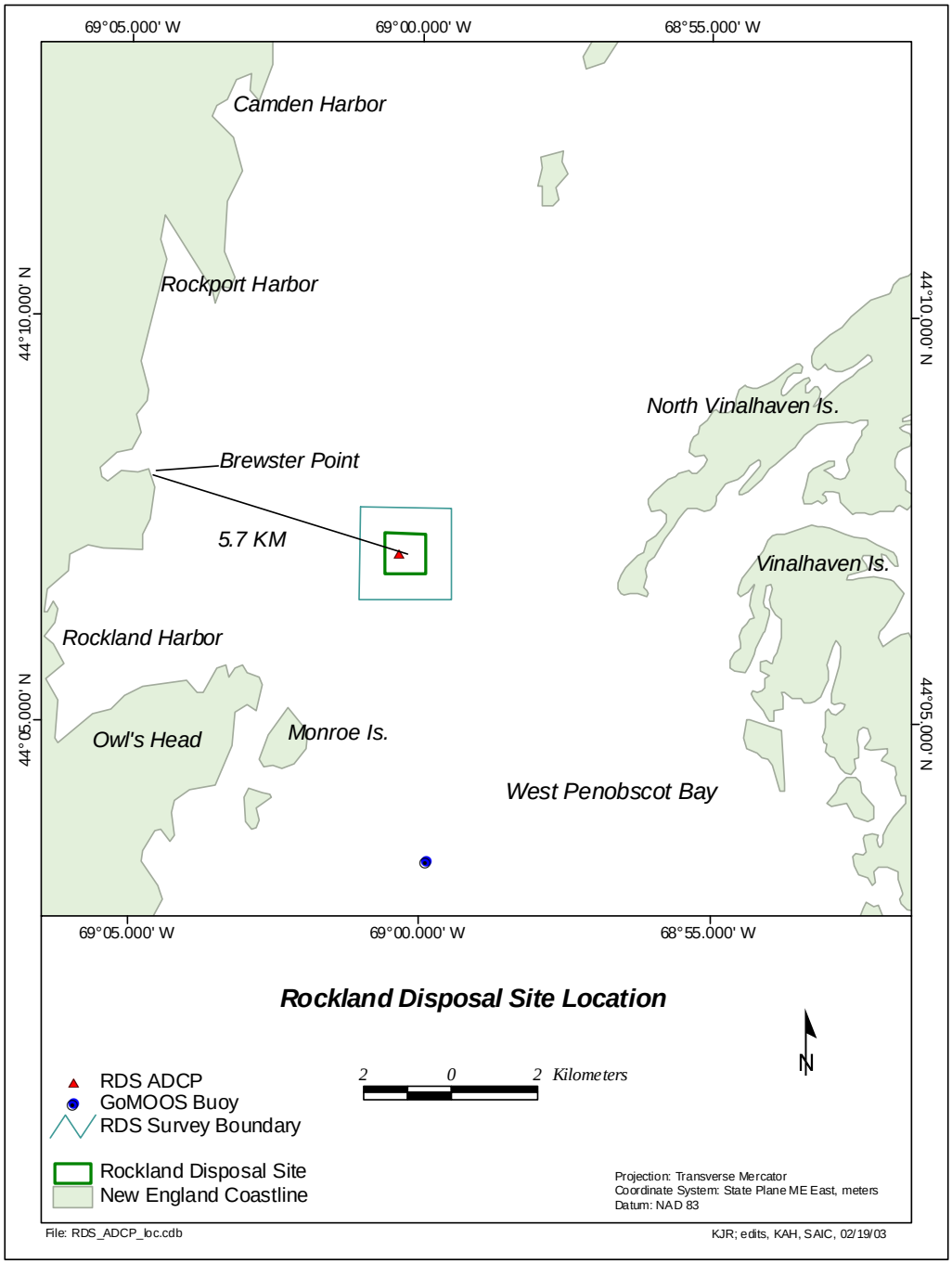

Figure 1-1. The location of the Rockland Disposal Site in West Penobscot Bay relative to the shorelines of the mainland and nearby islands

The objectives of the instrument deployment were to:

- Characterize currents at multiple depth levels from near bottom to the surface over a full 28-day tidal cycle, in an effort to understand the general flow characteristics, as well as maximum and minimum observed velocities throughout the water column.

- Measure near-bottom turbidity and relate any observed anomalies either to sediment resuspension or other processes.

- Perform harmonic tidal analysis on observed currents to separate major tidal constituents and determine phase relationships with depth throughout the water column.

- Analyze the residual flow (after the tidal currents had been subtracted) in the context of meteorological or freshwater forcing.

- Examine typical horizontal excursions from the deployment site on the timescales that dredged material plumes would remain suspended in the water column (a few hours or less).

- Obtain data on water property characteristics throughout the water column (density and turbidity) at the site during the deployment period of the moored array.

2.0 METHODS

2.1 Deployment Period

The instrument array deployment operation was performed aboard the M/V *Beavertail* on 4 August 2001, in coordination with survey activity at other dredged material disposal sites in the region. The array was placed at 44°07.093´ N, 69°00.388´ W in the western region of the disposal site, at a depth of approximately 70 m (Figure 2-1). This area of seafloor represented a historic dredged material deposit, which offered relatively flat bottom topography, as well as shallower depths to aid in the deployment and recovery of the instrument package (Figure 2-2).

Concurrent with the deployment, a vertical profile was made with a Seabird SBE 19-01 conductivity-temperature-depth (CTD) profiler, configured with a Seapoint optical backscatter (OBS) sensor, to characterize the water column temperature, salinity, and density properties, as well as background turbidity. In addition, a hydrocast was made using a 5 liter Niskin water sampling device to recover a water sample approximately 75 cm above the seafloor for total suspended solids (TSS) measurements.

After 32 days of data recording, the instrument array was successfully recovered from the RDS seafloor on 6 September 2001, aboard the F/V *Working Girl*. A hydrocast with the Niskin water sampler was collected at the end of the deployment period to compare the turbidity readings of the near-bottom sensor to TSS measurements. Hydrocasts were taken immediately before deployment and recovery to avoid bottom disturbance effects of the instrument array.

2.2 Navigation

Differentially-corrected Global Positioning System (DGPS) data in conjunction with Coastal Oceanographic's HYPACK® navigation and survey software were used to provide real-time navigation to an accuracy of ±3 m. A Trimble DSMPro GPS receiver was used to obtain raw satellite data and provide vessel position. The DSMPro is equipped with an integrated differential receiver to improve overall accuracy of the satellite data to the necessary tolerances. The US Coast Guard differential beacon broadcasting at 290 kHz from Penobscot, ME was utilized for real-time satellite corrections due to its geographic position relative to RDS. The DGPS data were ported to HYPACK® data acquisition software for position logging and helm display to aid in positioning the deployment vessel over the target location.

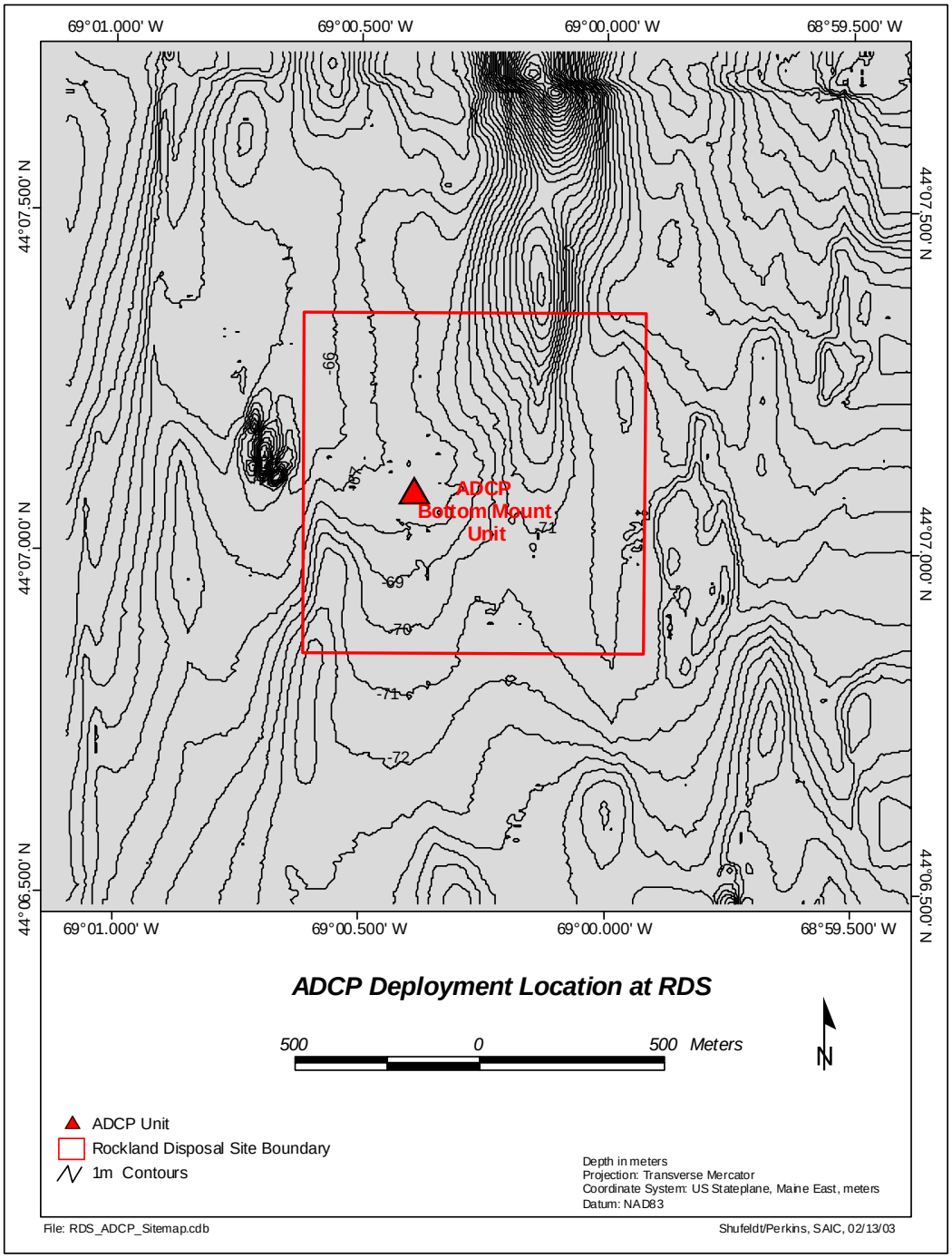

Figure 2-1. Location of instrument deployment at RDS relative to September 2000 bathymetry

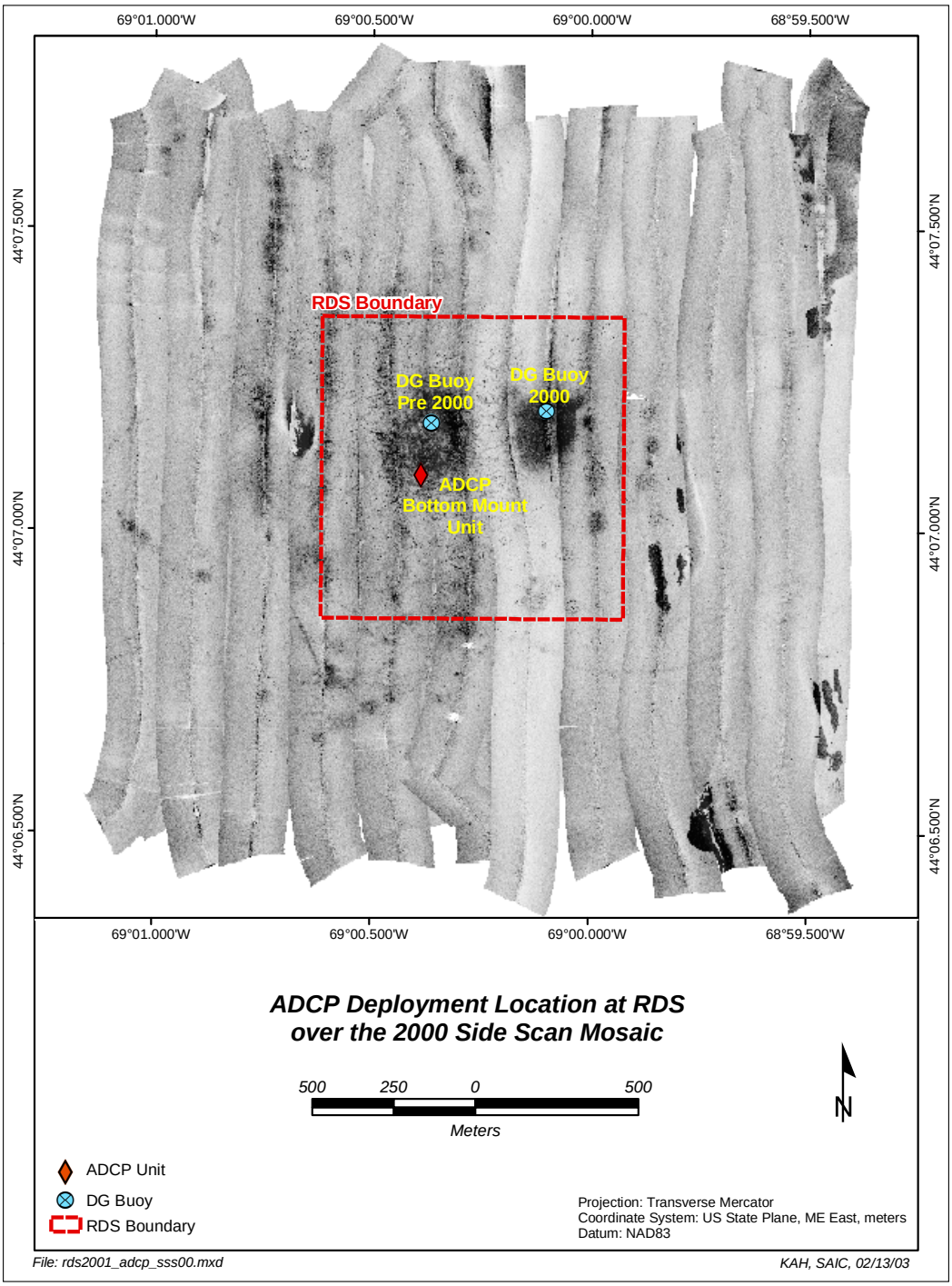

Figure 2-2. Location of instrument deployment location at RDS plotted over May 2001 side-scan sonar image of seafloor features

2.3 Current Meter and Turbidity Sensor Deployment

Based on the objectives of the oceanographic study, a multi-sensor bottom array was employed to accurately measure currents throughout the water column at RDS, as well as collect near-bottom current and turbidity data. A weighted quadrapod frame constructed of aluminum tubing was used as the basis of the instrument array. The frame was equipped with an upward looking RD Instruments 300 kHz Acoustic Doppler Current Profiler (ADCP) to measure water column velocities. A government-furnished side-looking Nortek Aquadopp acoustic Doppler current meter (ADCM) interfaced with a D&A optical backscatter (OBS) sensor was added to the array to measure near-bottom currents and turbidity. A Benthos model 866 acoustic release linked to a recovery float and line canister was mounted on the ARESS frame for retrieving the package (Figure 2-3).

The ADCP was mounted on one corner of the quadrapod frame, with the instrument head approximately 45 cm above the seafloor. The ADCP was configured to collect current velocity data (in north and east components) throughout the water column, and average the data into 2 m vertical bins for 40 depth levels (or 80 m) above the seafloor, in order to ensure that the entire water column was measured. The average value for each level represented the velocity recorded at the center of the vertical depth bin (e.g., a bin ranging from 2 to 4 m off the seafloor represents the velocity at 3 m). One velocity value was recorded for each vertical bin every 30 minutes based on 180 individual samples, or ADCP pings.

Near-bottom current velocities were recorded by the Aquadopp ADCM, which also was mounted on the quadrapod frame. The ADCM recorded three-dimensional velocities, as well as pressure and temperature at a level approximately 80 cm above the seafloor. The Aquadopp was configured to record an average velocity value every 30 minutes, with each value averaged from 60 individual samples collected at 30-second intervals (a lower number of samples than for the ADCP was selected to conserve battery life). An optical backscatter (OBS) sensor was interfaced with the Aquadopp ADCM to record near-bottom turbidity. The turbidity sensor was positioned approximately 110 cm above the seafloor. The OBS sensor sampled at the same interval and rate as the Aquadopp ADCM. A summary of the data recovered from all instruments is shown in Table 2-1.

2.4 Data Processing

Raw data acquired by the ADCP and Aquadopp current meters were converted into ASCII data files with software provided by the manufacturers. RD Instruments software was also used to determine the number of usable vertical bins of current data.

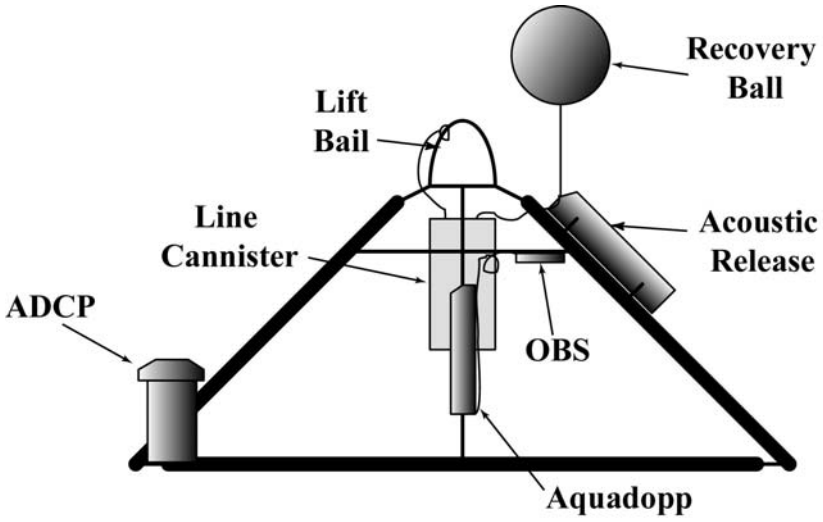

Figure 2-3. Photo and schematic diagram of the instrument array deployed at the Rockland Disposal Site

Table 2-1.

Moored Instrument Sampling Levels and Dates

Moored Instrument Type	Sampling Level (above seafloor)	Begin Date and Time (GMT)	End Date and Time (GMT)
ADCP	9-69 m	8/4/2001 14:00	9/6/2001 12:30
Aquadopp	80 cm	8/4/2001 14:00	9/6/2001 12:30
OBS	110 cm	8/4/2001 14:00	9/6/2001 12:30
Pressure	80 cm	8/4/2001 14:00	9/6/2001 12:30
Temperature	80 cm	8/4/2001 14:00	9/6/2001 12:30

The software provided by Seabird Electronics automatically converted turbidity values recorded by the OBS sensor on the CTD instrument into Formazin Turbidity Units (FTU). A calibration provided by the manufacturer of the D&A OBS sensor (on the moored array) was used to convert these data to Nephelometric Turbidity Units (NTU). In practice, NTU and FTU can be interchanged readily. All data were then imported into Mathworks MATLAB computational software for processing and analysis.

Basic processing of the current records consisted of converting the U (east) and V (north) components of velocity recorded by each instrument into a vector magnitude and direction. A deployment mean magnitude and direction composed of each component mean was calculated for each depth bin of the ADCP data and for the single depth of the Aquadopp data. In addition, a mean speed independent of direction was calculated from the vector magnitude for each observation.

2.5 Harmonic Analysis

A harmonic tidal analysis was performed to extract information on the tidal nature of the currents observed at the site. The harmonic analysis generated a best fit of the current meter data through a Fourier synthesis utilizing predetermined frequencies of tidal forcing.[1]

The harmonic analysis was performed on both the north and east components of the current record, generating an amplitude and phase of each Fourier constituent. Using these parameters, a tidal ellipse, or hodograph, can be generated for each tidal constituent at each depth level. The tidal ellipse represents the trace of the tip of a current vector as it rotates through one period of the given constituent (Figure 2-4). Four parameters result from this calculation: 1) the major axis amplitude in $cm \cdot s^{-1}$, 2) the minor axis amplitude, 3) the inclination of the major axis (rotated counterclockwise relative to east), and 4) the phase of the constituent relative to the beginning of the dataset, as well as the errors associated with each calculation. Thus, one can examine how the tidal currents rotate with depth and any associated phase changes with depth.[2] In addition to ellipse parameters, the harmonic analysis package calculated the variance associated with raw data, the tide fit, and the residual calculation resulting from the subtraction of the two. As such, one is given a percentage of the current velocities that are tidal.

[1] The tidal analysis was performed with routines written for Matlab by Rich Pawlowicz at the Institute of Ocean Sciences in British Columbia, based on algorithms formulated by Foreman (1977).

[2] A Matlab routine written by Zhigang Xu at the Bedford Institute of Oceanography was utilized to plot the ellipses.

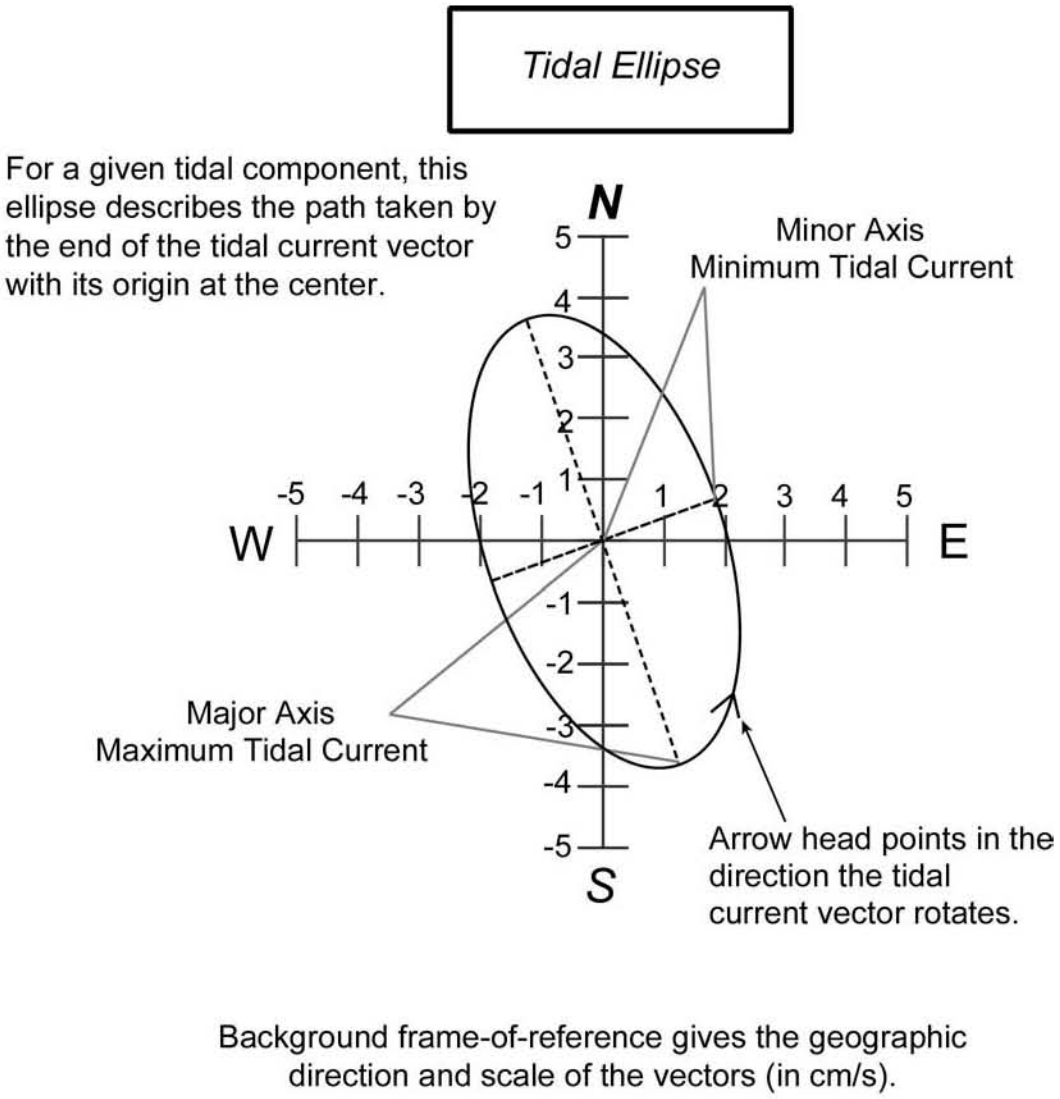

Figure 2-4. Diagram of a tidal ellipse describing the associated parameters

2.6 Residual Analysis

Examination of low frequency, non-tidal changes in water column currents was undertaken using three methods. The first approach was to examine long-term mean currents, which was addressed in Section 2.4. The next method was to apply a low-pass filter to the velocity data, which removed any variability in the currents that occurred on a timescale shorter than the filter length. For this analysis, a 30-hour, second order low-pass Butterworth filter was applied, to ensure that all major tidal frequencies were removed (excepting, of course, Spring-Neap and monthly). The filter was run backwards as well as forwards through the dataset to avoid any phase changes. This allowed the velocity data to be examined on a synoptic timescale, in the context of potential forcing from winds and freshwater discharge.

After generating a record of purely tidal currents for the dataset, the tidal current record can be subtracted from the raw data to obtain the residual, or non-tidal current component. The advantage of this method is that the magnitude of the residual flow was not reduced by the filtering process, and any potential wind and/or wave forcing that might have occurred on a timescale shorter than the filter cutoff is not removed.

2.7 TSS Analysis

Water samples were taken at the instrument location immediately following deployment and prior to a recovery at a level of approximately 75 cm above the seafloor. These samples were analyzed for the volume of suspended material per volume of water sample. The procedure consisted of filtering 200 ml of sample with a pre-weighed glass fiber filter, drying the filter and residue, and weighing the dried sample. The weight of the filter was then subtracted from the dried weight to obtain the mass of suspended material for the volume filtered, giving a total suspended solids value in $mg \cdot l^{-1}$ (NCASI Technical Bulletin 1977).

3.0 RESULTS

3.1 Water Column Mean Currents

Both current meters (ADCP and ADCM) that were deployed on the bottom frame acquired good quality data for the entire 32-day period. Reliable data from the ADCP extended from 3 to 61 m above the seafloor (or 9 to 67 m water depth) in approximately 70 m of water. Although the instrument used had the capability to penetrate the entire water column, data near the surface is typically corrupted by signal interference caused by surface waves. Thus, consistent and reliable ADCP data began 9 m below the surface. Data were archived in terms of a north-south component and an east-west component, and the direction was corrected for the local magnetic variation. From these measurements, it was possible to compute a magnitude and direction of the velocity for each current measurement.

Time series of current speed and direction from three depth levels (9 m, 29 m, and 49 m) as well as from the Aquadopp ADCM at approximately 69 m depth (80 cm off the seafloor) are presented in Figure 3-1. The most prominent feature in the velocity record was associated with the semidiurnal tide. This is observed as steady increases and decreases in current speed with time in response to the rising and falling tide. As the site lies in the west passage of Penobscot Bay, currents were expected to be primarily bi-directional, or northeast-southwest in this location. This was evident in the velocity records from deeper within the water column, where the current direction switched relatively quickly from a southward to a northward direction (from ebb to flood), and vice versa. The current at 9 m was primarily bi-directional as well, although the effects of winds and other high frequency processes in the upper water column were evident at times. Correlations with meteorological events and river discharges could be computed for these periods, but such analyses are beyond the scope of this study.

Mid-water column currents were the strongest, reaching 45 $cm \cdot s^{-1}$ at 49 m depth. It is interesting to note that velocities were higher on average in the center of the record at each depth level. This corresponds to the spring-neap tidal signal, with a period of 14 days. Peak velocities were as much as 20 $cm \cdot s^{-1}$ higher, or twice as high during the spring portion of the record (full/new moon) than the neap portion (1/4 moon). The record length was sufficient for a harmonic analysis to calculate the magnitude of the various tidal constituents as presented later.

Additional current data for the deployment period within the West Passage (WP) of Penobscot Bay were obtained through the University of Maine Gulf Of Maine Ocean Observing System (GoMOOS). The position of the GoMOOS WP buoy is plotted in

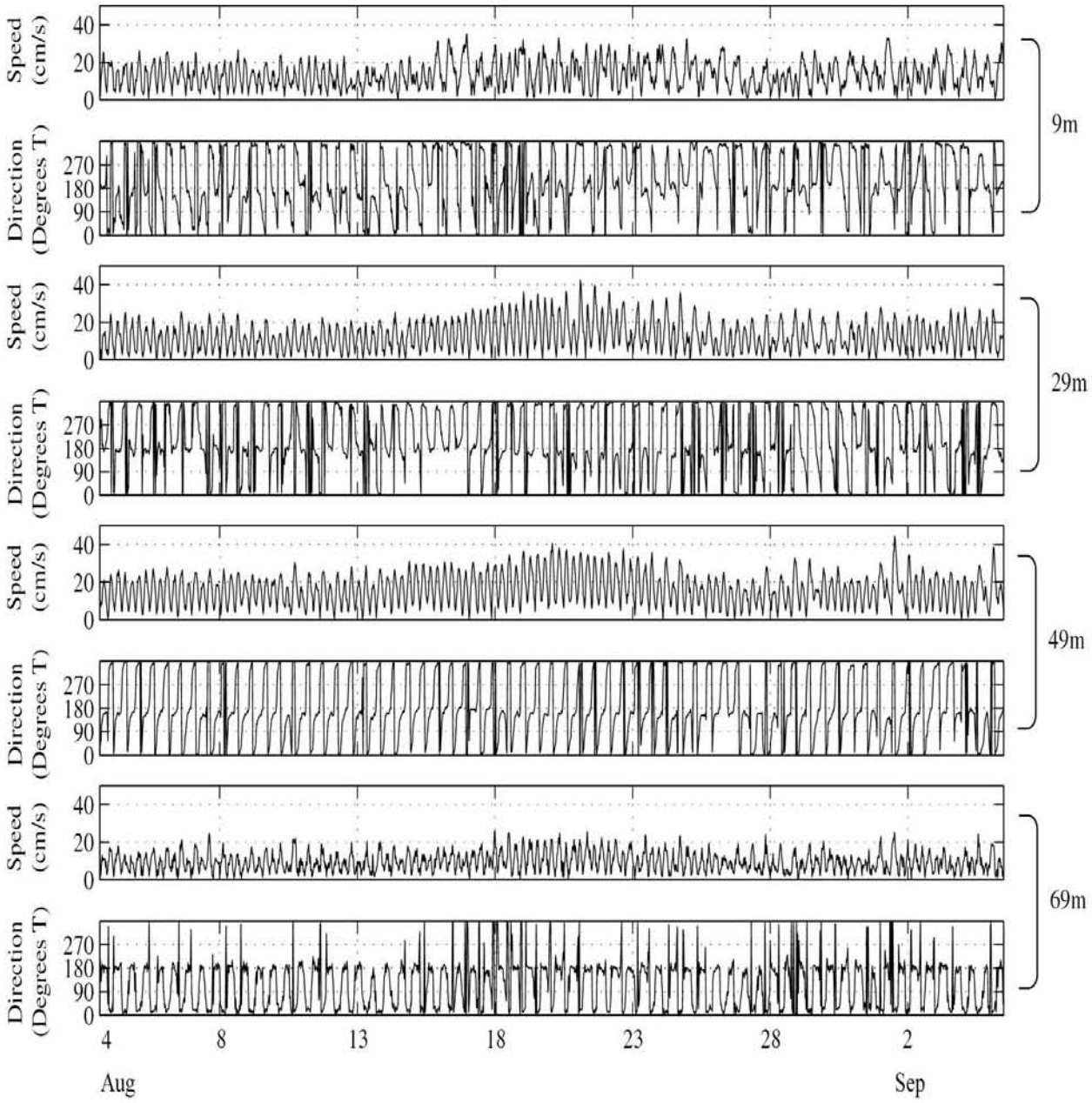

Figure 3-1. Time series of unfiltered half-hour current speed and direction for depth levels of 9 m, 29 m, and 49 m from the ADCP and at 69 m from the Aquadopp

Figure 1-1. The buoy contains an ADCP oriented downwards to measure water column currents and an ADCM to measure near-surface currents. The buoy also contains meteorological instruments to measure wind speed and direction and air temperature. Although a full treatment of the GoMOOS data is beyond the scope of this study, a quick comparison showed that similar characteristics in the currents were observed at this site during the study period.

For numerical modeling purposes it is necessary to examine the current flow in the context of long-term trends. First, a mean of the U and V current velocity components was computed separately for the entire record length, and a mean magnitude and direction was then constructed (referred to as the vector mean). These values then represented the mean horizontal drift or particle transport pathway over the long term. The results from the analysis are plotted in Figure 3-2 for the entire water column, and presented in Table 3-1 for the same depth levels represented in Figure 3-1, along with minimum and maximum values for each depth. The vector means showed a fairly consistent magnitude profile of very low values (< 3 cm·s^{-1}) through the water column, with a slightly lower value recorded 9 m below the surface. Such low values are calculated because the primarily bi-directional tidal currents tend to offset each other. Mean direction indicated northward mean flow at 29 and 9 m depths, northeastward mean flow deeper in the water column, and eastward flow at the bottom. The preferred north-northeastward direction corresponded well with the isobaths and geometry in the region of the disposal site, with flow tending along isobaths.

The second method used to examine long-term differences between depth levels was to calculate a vector magnitude for each record from the U and V components, and then compute a mean speed (Figure 3-2; Table 3-1). This scalar quantity represented the speed that might be encountered at a given depth level at any point in time, independent of current direction. Mean speeds tend to be higher than vector means, as there are only positive values given for the magnitude. This is in contrast to the vector mean computation, where southward and eastward negative values tend to offset or cancel northward and westward values. Thus, mean speeds are often used as a worst case scenario for disposal plume modeling. Interestingly, mean speeds are slightly higher at depth (16.1 cm·s^{-1} at 49 m) than in the upper water column (13.5 cm·s^{-1} at 19 m).

Longer-term velocity trends can also be examined by plotting a histogram of the direction of each current measurement on a compass rose plot. Figure 3-3 presents the compass rose diagrams that were generated for the previously discussed depths of 9, 29, 49, and 69 m. Here, the bi-directional nature of the currents was even more pronounced, with most measurements clustered in a north-south general direction, with a slight bias to

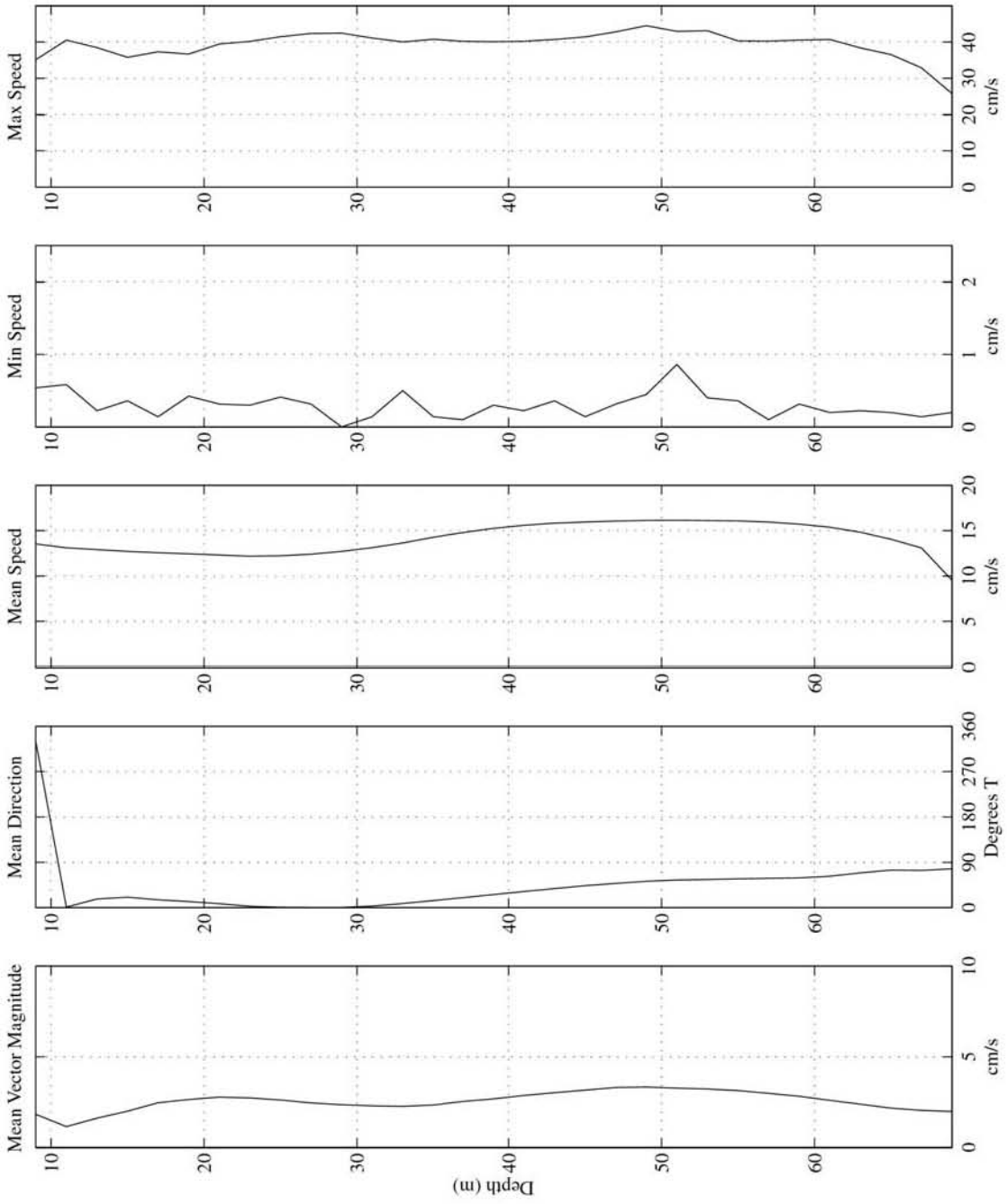

Figure 3-2. Vertical profile of long-term mean vector magnitude and direction as well as mean speed, minimum speed, and maximum speed as recorded by the ADCP and near-bottom Aquadopp (bottom data level)

Table 3-1.

Statistical Results from Current Records Acquired at
Four Depth Levels at the Rockland Disposal Site

Depth Level (m)	Mean Vector Magnitude ($cm \cdot s^{-1}$)	Mean Direction (°T)	Mean U ($cm \cdot s^{-1}$)	Mean V ($cm \cdot s^{-1}$)	Mean Speed ($cm \cdot s^{-1}$)	Maximum Speed ($cm \cdot s^{-1}$)
9	1.8	330.5	-0.9	1.6	13.5	35.1
29	2.4	0.7	0.0	2.4	12.7	42.4
49	3.3	52.4	2.6	2.0	16.1	44.5
69	2.0	95.4	2.0	-0.2	9.5	25.8

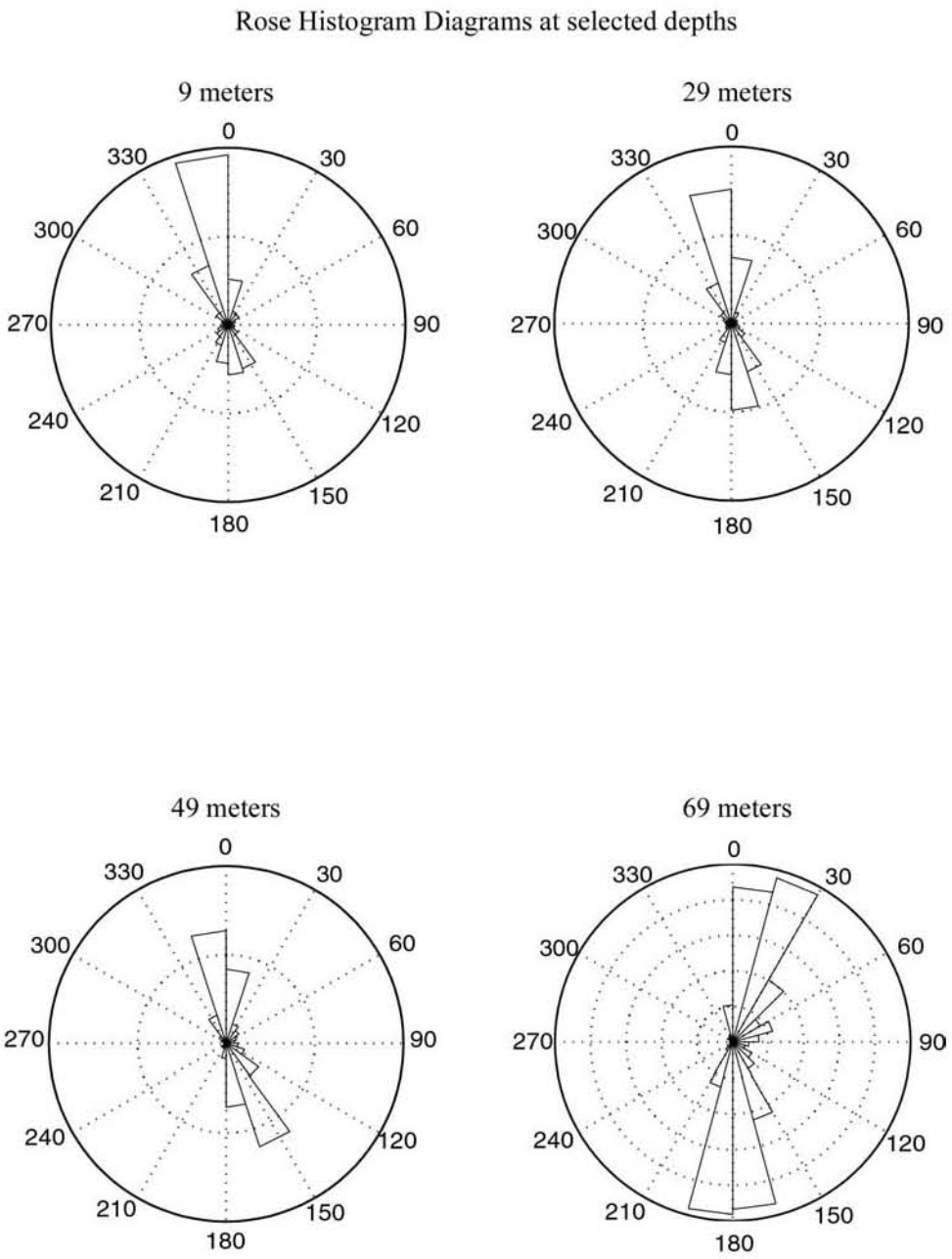

Figure 3-3. Current rose histograms for depth levels of 9 m, 29 m, and 49 m from ADCP data, and 69 m from Aquadopp data. Bars represent frequency in 15-degree bins distribution from 1577 half-hour measurements acquired from 4 August to 6 September 2001.

the north in the upper half of the water column. Near the surface, currents were more focused in the northward direction than at any other level, which is most likely a result of the prevailing southerly winds in this region at this time of year. Bottom currents were oriented more northeast-southwest than the rest of the water column. At the bottom, it is important to note that while the vector mean direction for the entire record was to the east, the rose diagrams indicated that at any given time, either a northeastward or southwestward flow were more likely, depending on the stage of the tide.

3.2 Tidal Currents

3.2.1. Variance of Raw, Tide Fit and Residual Currents

In calculating a tidal fit for the current record, the harmonic analysis package calculates the variance (the square of the standard deviation) from the raw time series, the tidal fit generated, and the residual currents that result from the subtraction of the tide fit from the raw data. In doing so, one can obtain a percentage of the record that is tidal and subsequently a percentage that is residual. As there were both east-west and north-south velocity components, the variance was calculated for each. As the results presented in Table 3-2 indicate, the currents at the site are primarily tidal in nature. In addition, the north-south currents were even more tidal (95% for most of the water column) than the east-west currents.

3.2.2. Tidal Ellipse Parameters

From the calculation of the magnitude and phase of the tidal harmonic constituents tidal ellipses for the major tidal lines can be constructed. The results from the three most significant constituents (M_2, N_2 and S_2) at selected depths are presented in Tables 3-3 to 3-5, and ellipses for the M_2 constituent are plotted in Figure 3-4 for selected depth levels. The M_2 tide, typically the largest with a period of 12.42 solar hours, is the direct result of lunar gravitational forcing as the earth rotates, whereas the S_2 tide, with a period of 12.00 solar hours, is the direct result of solar gravitational forcing. The N_2 tide on the other hand, with a period 12.66 solar hours, is the result of non-linear interaction of the other two constituents. Tabular results from other major constituents can be found in Appendix B. The lunar M_2 and N_2 constituents were greatest at mid-to-lower depths (approximately 22 $cm \cdot s^{-1}$and 6 $cm \cdot s^{-1}$ respectively), whereas the solar S_2 constituent was greatest closer to the surface (at approximately 3 $cm \cdot s^{-1}$). All ellipses were highly rectilinear, that is, the ratio of the minor axis to major axis is low. In fact, there was practically no minor axis in the near-bottom currents at all. As the site lies in a relatively narrow passage, this was not a surprising result. The fact that tidal currents were stronger

Table 3-2.

Variance of Raw, Predicted, and Residual Currents
Calculated by Harmonic Analysis Package

Depth	U (cm/s)	Upredict (cm/s)	Uresidual (cm/s)	Upercent	V (cm/s)	Vpredict (cm/s)	Vresidual (cm/s)	Vpercent
9 m	29.48	10.67	18.81	36.20	200.41	137.00	63.40	68.40
19 m	24.46	14.20	10.26	58.00	172.58	163.13	9.45	94.50
29 m	16.42	7.89	8.53	48.00	198.59	187.06	11.53	94.20
39 m	25.78	19.17	6.61	74.40	267.47	254.82	12.65	95.30
49 m	29.51	23.92	5.59	81.10	287.87	276.00	11.87	95.90
59 m	13.47	8.02	5.44	59.60	294.15	281.33	12.82	95.60
69 m	25.52	18.94	6.59	74.20	87.33	78.70	8.63	90.10

Table 3-3.

Ellipse Parameters for the M_2 Tidal Constituent Generated by Harmonic Analysis
(Major and Minor Axis Values in $cm \cdot s^{-1}$, Inclination and Phase in Degrees)

Depth	Major	Error	Minor	Error	Inclination	Error	Phase	Error
9 m	15.35	1.03	1.13	0.78	94.07	2.92	356.10	3.87
19 m	17.40	0.53	2.72	0.78	100.67	2.64	8.59	1.82
29 m	18.58	0.54	0.36	0.73	99.03	2.25	9.69	1.65
39 m	22.07	0.59	-2.83	0.46	101.91	1.24	14.23	1.56
49 m	23.08	0.52	-3.62	0.69	103.03	1.77	12.21	1.36
59 m	22.57	0.48	-3.08	0.62	93.86	1.62	4.37	1.26
69 m	13.12	0.29	0.02	0.42	64.70	1.84	356.76	1.27

Table 3-4.

Ellipse Parameters for the N_2 Tidal Constituent Generated by Harmonic Analysis (Major and Minor Axis Values in $cm \cdot s^{-1}$, Inclination and Phase in Degrees)

Depth	Major	Error	Minor	Error	Inclination	Error	Phase	Error
9 m	2.64	1.01	0.45	0.81	70.80	18.42	319.27	22.72
19 m	4.49	0.52	1.09	0.78	98.86	10.76	336.73	7.55
29 m	4.89	0.55	-0.25	0.72	107.47	8.42	341.61	6.49
39 m	6.15	0.59	-1.64	0.47	105.31	4.93	353.12	6.00
49 m	6.27	0.52	-1.25	0.69	102.98	6.64	348.07	5.15
59 m	5.76	0.48	-0.90	0.62	97.19	6.38	336.14	5.02
69 m	3.42	0.27	-0.06	0.44	71.50	7.29	331.48	4.52

Table 3-5.

Ellipse Parameters for the S_2 Tidal Constituent Generated by Harmonic Analysis (Major and Minor Axis Values in $cm \cdot s^{-1}$, Inclination and Phase in Degrees)

Depth	Major	Error	Minor	Error	Inclination	Error	Phase	Error
9 m	1.89	0.99	-0.07	0.83	65.32	25.19	78.46	30.27
19 m	3.43	0.52	-0.26	0.78	81.83	13.22	45.95	8.85
29 m	3.35	0.56	-0.38	0.71	111.28	12.36	71.10	9.84
39 m	3.17	0.57	-0.74	0.49	119.41	9.79	84.11	11.05
49 m	2.88	0.54	-0.26	0.68	110.94	13.67	68.73	10.93
59 m	3.08	0.49	-0.39	0.62	101.15	11.78	57.50	9.34
69 m	1.79	0.27	-0.04	0.44	73.20	14.03	52.66	8.50

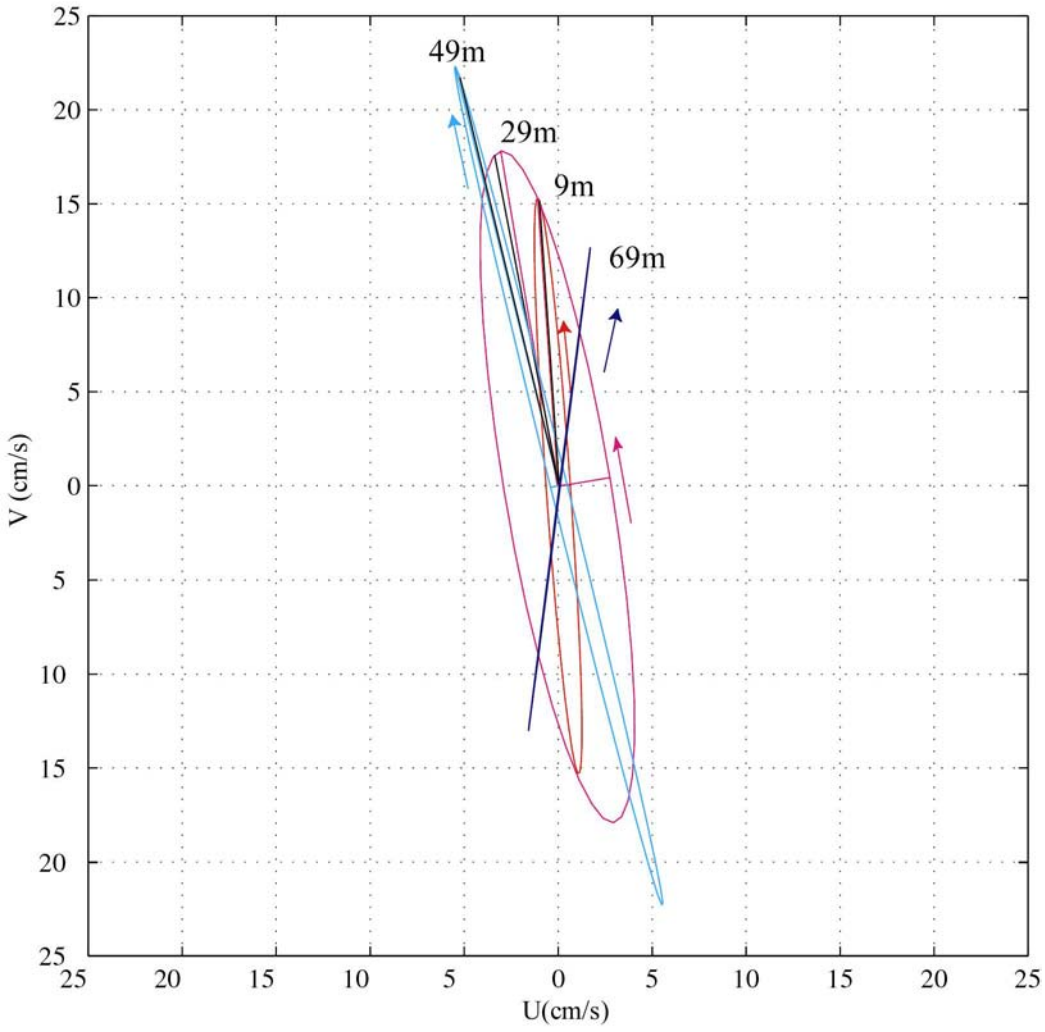

Figure 3-4. Tidal ellipses for M_2 constituent as calculated by harmonic analysis from ADCP depth levels 9 m (red), 29 m (magenta), 49 m (cyan), and from the Aquadopp at 69 m (blue). The black line for each ellipse represents the current vector at time t_0 at the beginning of each dataset. Arrows indicate direction of vector rotation through the tidal cycle for each depth level.

in the mid-to-lower water column concurs with the aforementioned mean speed calculations. The sense of rotation, that is, whether the currents rotate clockwise (CW) or counterclockwise (CCW) through a tidal period is given by the harmonic analysis as well, and is represented in Figure 3-4 as an arrow for each ellipse. It is interesting to note that rotation is CCW for all depth levels presented except for the mid-depth level at 49 m. For such rectilinear tidal currents, however, the rotational sense may not be easily distinguished by the harmonic analysis, and therefore these results may not be trustworthy.

It is interesting to note that the inclinations of the major axes were primarily aligned for the three major constituents, predominantly to the north and northwest (90° rotated CCW from east gives an inclination of north). Again, this was due to the topographic control that the constriction of the passage induced. In addition, inclinations of the major axis tended to rotate CCW from surface to mid-depth, and then clockwise again from mid-depth to bottom. Although it appeared to be a sudden change from the 49 m depth level to the 69 m level, plotting the ellipses from the remainder of the ADCP data revealed that this change is gradual.

The phases of different constituents are not as well aligned, however, either between constituents or between depth levels. In particular, the bottom and near-surface tides were earlier in phase than the mid-water column tides for the M_2 constituent. Thus, the bottom and surface tidal current would tend to change direction before the mid-water column, by as much as 40 minutes, as the phase difference indicated. This would mean that a particle falling in the water column might experience tidal currents of different directions at the time of tide change. In addition, it should be kept in mind that the various constituents having differing frequencies, phases, and inclinations could at times add to create a stronger current, and at other times subtract to give a reduced tidal current.

3.3 Residual Currents

It is of interest to examine the current record in the context of low frequency, sub-tidal forcing. The first method was to filter the velocity data with a low-pass filter in order to remove the high frequency variability (on a timescale shorter than the major tidal constituents). Figure 3-5 illustrates 30-hour low-pass filtered currents from the four depth levels of 9 m, 29 m, 49 m (all from ADCP) and 69 m (from Aquadopp).

The first observation made was that the low-frequency current vectors for each depth level corresponded well with the long-term mean, with northerly mean currents at 9 m and 29 m depth, northeasterly mean currents at 49 m depth and easterly mean currents at the near-bottom (69 m) level. Sub-tidal velocity events were strongest near the surface,

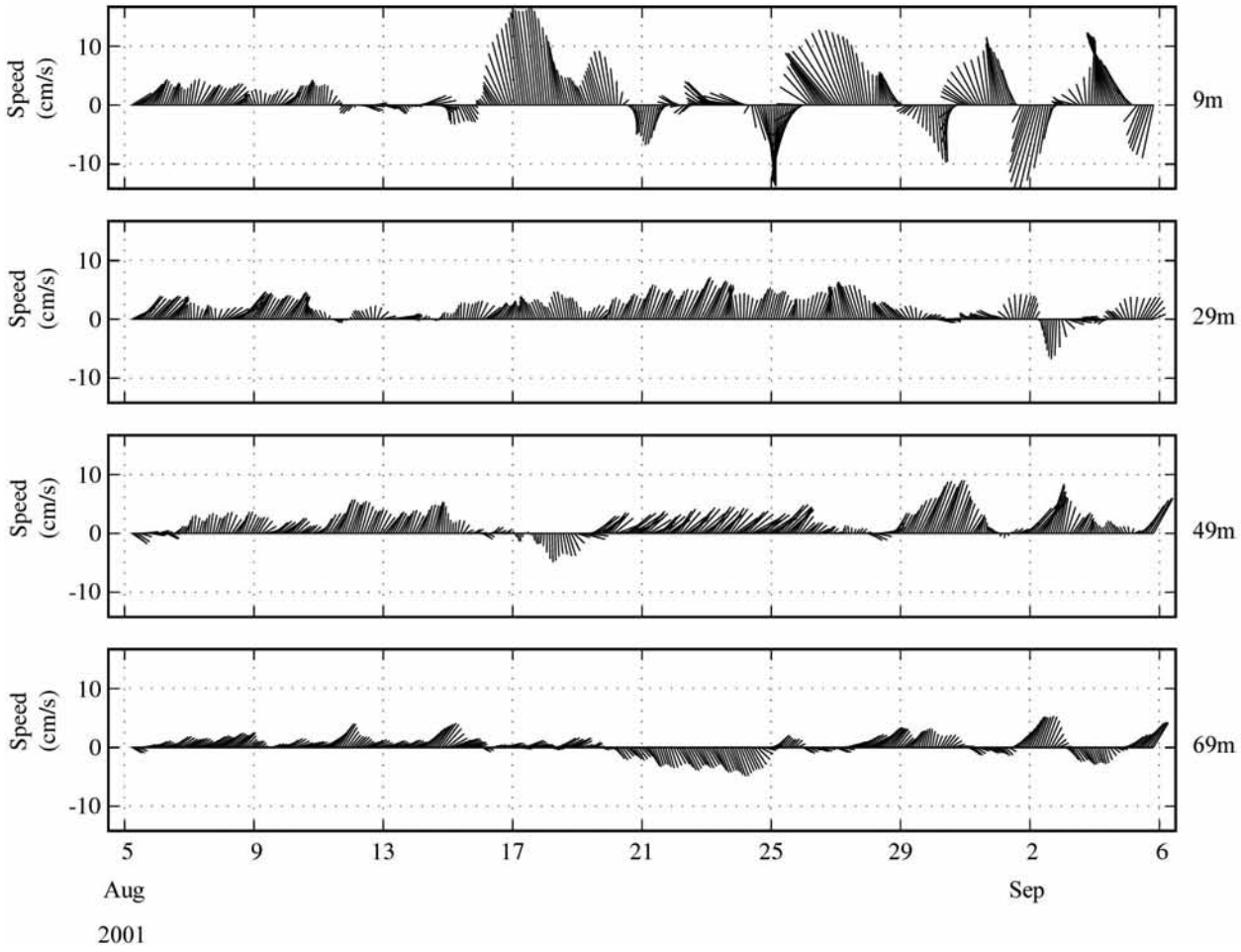

Figure 3-5. Vector plot of 30-hour low-pass filter currents (2 hour sample for viewing ease) for the entire deployment from ADCP depth levels 9 m, 29 m, 49 m and the Aquadopp at 69 m

and typically occurred on a 3 to 5 day timescale corresponding with the synoptic timescale of weather systems in the region. Wind records for the period of deployment were acquired from the University of Maine's GoMOOS real-time coastal observation buoy F in the West Penobscot Bay at a position of 44°03.30´N, 068°59.88´W (Figure 3-6), which lies approximately 7 km almost due south.

Based on the wind and current records for the deployment period, it appeared that low-frequency near surface currents mimicked the meteorological trends (Figure 3-6). There also appeared to be a phase lag in the response of the lower water column to events that take place at the surface. This response of lower depth levels may have been in the opposite manner from the surface, as the near bottom showed average southward currents from 20 to 25 August (Figure 3-6), after a large northerly event in the surface waters from 16 to 20 August. Without a more detailed statistical analysis between the datasets, however, it is difficult to postulate such relationships with confidence. Nevertheless, variation in the low frequency currents at depth also followed a 3 to 5 day periodicity, indicative of the meteorological forcing.

The last method of examining residual flow was to subtract the tide fit generated by the harmonic analysis from the raw data to construct a residual current. In doing so, we obtained an actual value of the current that is not associated with tidal forcing at any given time in the record. The residual currents are plotted in Figure 3-7 for the same depth levels as had been shown for the 30-hour low-pass filtered currents in Figure 3-5. Although the general trends in the two different residual calculations agreed well, the tide-subtracted current showed stronger magnitudes for a given velocity event. In addition, the directions calculated in this method are more erratic than the smoothed 30-hour filtered current, demonstrating the higher frequency variability that was removed in averaging. Thus, a tide-subtracted residual current was more accurate in determining the absolute magnitude of the water column response to a given wind event, independent of the underlying tidal currents.

3.4 Near-Bottom Pressure, Temperature and Turbidity

In addition to velocity, the ADCM recorded the water temperature and pressure at 80 cm off the seafloor. Data from the OBS turbidity sensor was stored in the Aquadopp memory as well. These data are presented in Figure 3-8, along with the velocity data recorded by the Aquadopp at 69 m depth (also presented in Figure 3-1) for comparison. Currents at the bottom were primarily bi-directional with the incoming and outgoing tides. Pressure data also demonstrates the predominance of the lunar semidiurnal tide (period of 12.42 hours), with an average value of 69 m above the instrument, giving an average water depth of approximately 70 m (as the instrument was situated 80 cm above the seafloor).

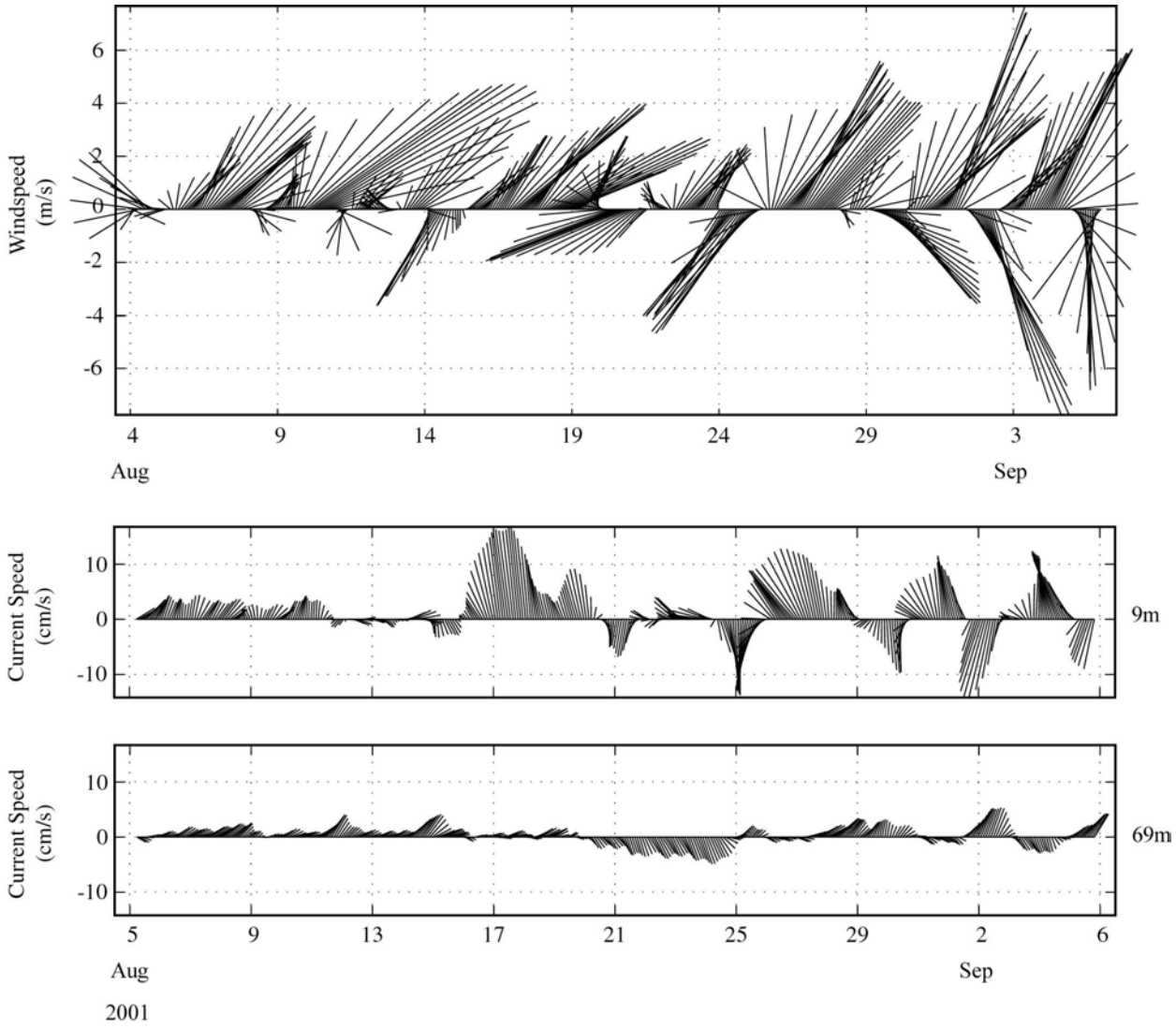

Figure 3-6. Vector plot of 12-hour low-pass filter wind data (4-hour sample for viewing ease) collected at University of Maine GoMOOS real-time buoy in West Penobscot Bay, as well as 30-hour low-pass filter surface currents from the ADCP and near-bottom currents from the Aquadopp

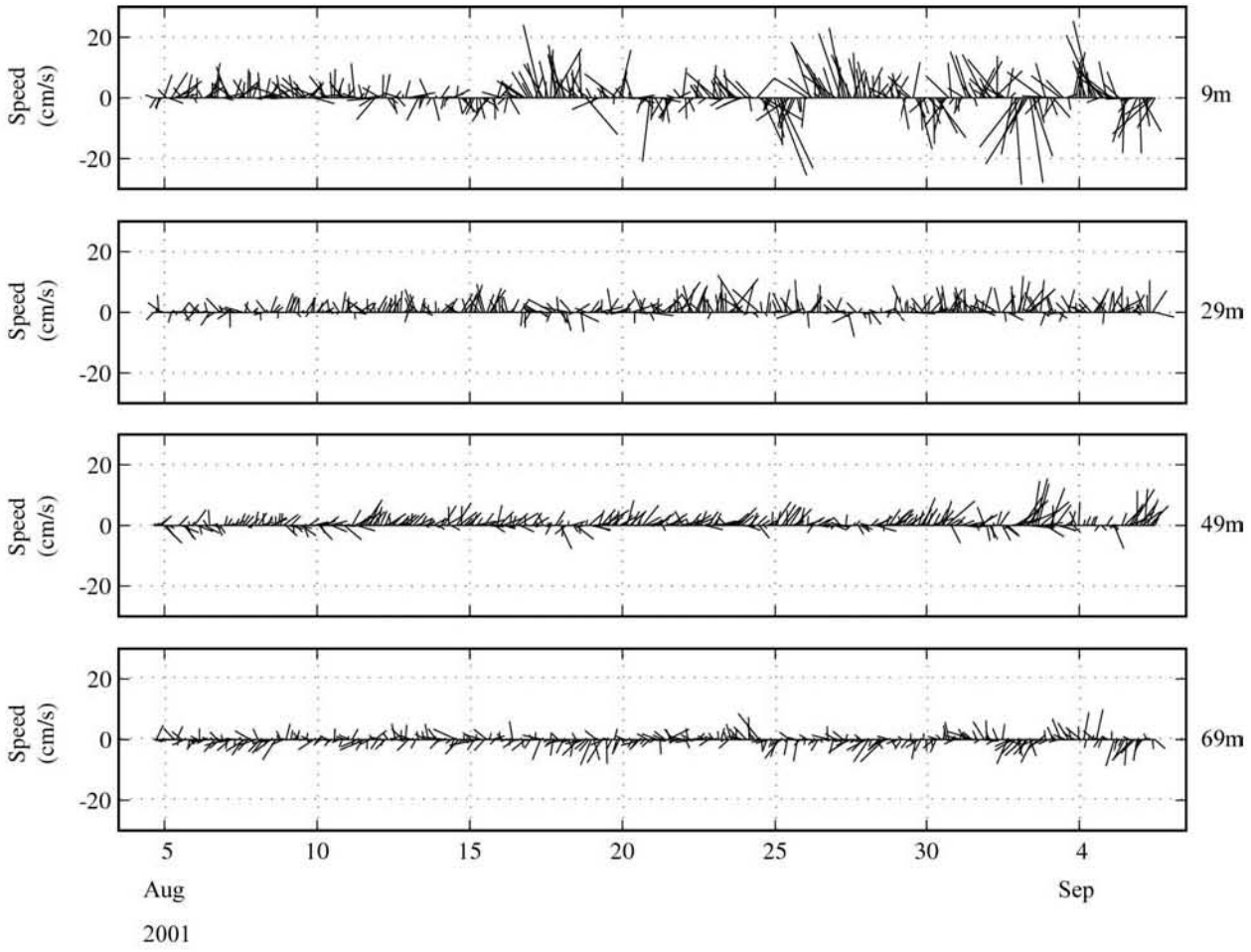

Figure 3-7. Vector plot of tide subtracted residual currents (2-hour sample for viewing ease) for the entire deployment from ADCP depth levels 9 m, 29 m, 49 m and the Aquadopp at 69 m

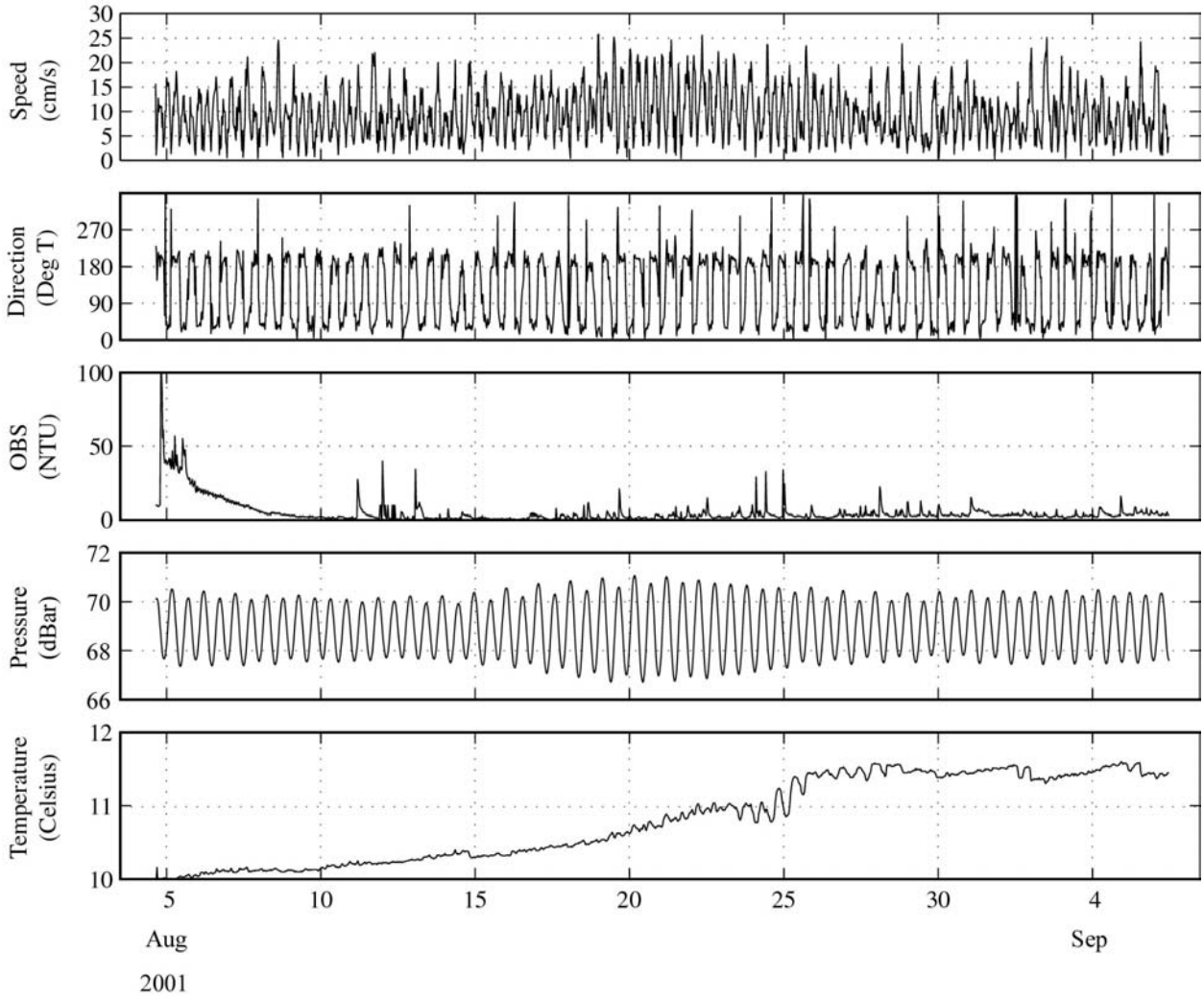

Figure 3-8. Time series of near-bottom current (speed and direction), turbidity, pressure and temperature data collected at 69 m depth in the Rockland Disposal Site. Data were sampled every half hour from an average of measurements over the sampling period.

The most obvious trend in the pressure record was that of the M_2 lunar semidiurnal tide. The tidal range from low to high tide varied from just over 1 m to almost 4 m, depending on the time of the month. This variation in the tidal range was clearly due to the spring-neap modulation of the semidiurnal component. This leads to a 1 m difference between the higher high tide at spring (as on 21 August) and neap (as on 4 September). As mentioned previously, this had notable consequences on the velocities recorded. A harmonic tidal analysis was performed on the pressure record as well, and the difference in variance between the raw data and the tide fit suggest that the signal was more than 99% tidal. Water temperature over the deployment period increased at the bottom by 1.5° C (from 10°C to 11.5°C), which was to be expected in late summer in this region. A maximum temperature of approximately 11.5° C was reached on 26 August after which temperature fluctuated around this value for the remainder of the deployment (10 days).

The moored, near-bottom turbidity data were generally reliable but contain some irregularities. The record began with relatively high turbidity values (up to approximately 50 NTU and less), which gradually decreased over a few days (Figure 3-8). Given that the TSS sample from the beginning of the deployment showed only trace amounts of suspended solids (see next section) and that the CTD/OBS cast taken upon deployment gave readings of approximately 3 FTU at the bottom, it is likely that the high values in the first few days of the moored turbidity data record were an anomaly. The most plausible explanation is that the instrument was temporarily affected by the sudden temperature change, or that it was fouled by sediment or organic matter that eventually cleared itself. An extremely large spike is noted in the evening of 11 August, with values as high as 2000 NTU. It is not possible that this peak represents sediment resuspension, as there is no corresponding peak in the velocity record. Since the sensor emits light and measures the intensity of the return, it is susceptible to any solid matter that passes in within 5 cm of the sensor head. Thus, it has been determined that this unusual spike in the record was most likely the result of the sensor being temporarily fouled by drifting seaweed or other solid matter.

Otherwise the turbidity data generally showed low background values of 0–10 NTU, with intermittent short increases of low magnitude, typically less than 30 NTU. These small events are short in duration as well, generally lasting two hours or less. There did not appear to be any corresponding velocity increases with the high turbidity events, suggesting that they do not represent local resuspension events. It is more likely that these brief elevated turbidities were the result of the advection of more turbid waters from another source outside the boundaries of the disposal site.

In addition to moored time series data on near-bottom temperature and turbidity, a vertical hydrocast with a CTD profiler equipped with a turbidity sensor was taken at the beginning of the deployment. The data are presented in Figure 3-9, with temperature,

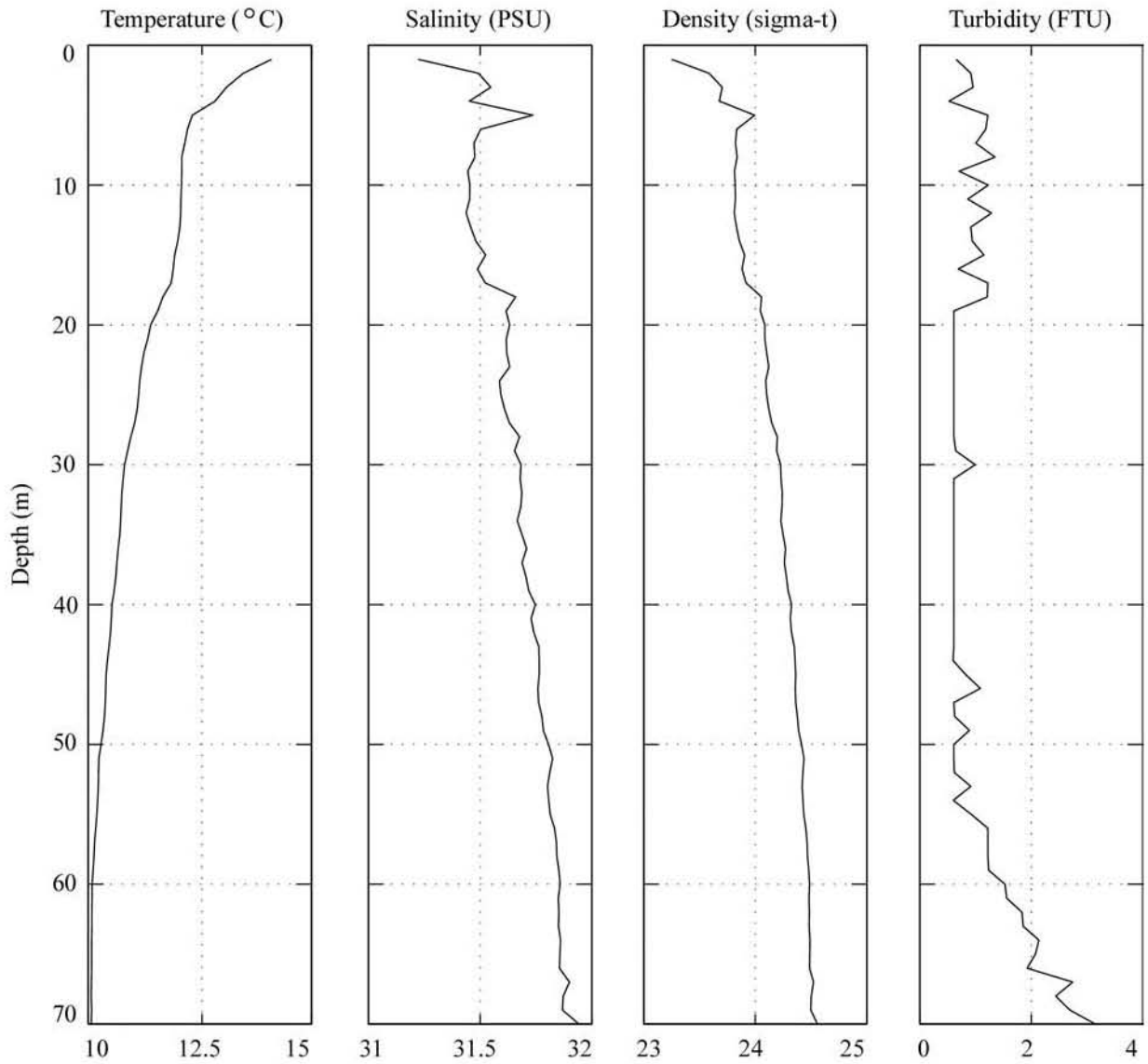

Figure 3-9. Vertical profiles of temperature, salinity, density, and turbidity acquired within the Rockland Disposal Site on 4 August 2001

salinity, density, and turbidity profiles plotted versus depth. Temperature shows the typical thermal stratification that develops in the summer months in this region, with a 4.5° C difference from surface to bottom. Salinity also exhibited some vertical structure, although not very acute, with less than one PSU difference from surface to bottom. The resultant density profile (in sigma-t units) demonstrated a relatively gradual increase, from approximately 23.25 to 24.5 $kg \cdot m^{-3}$ from surface to bottom. Turbidity data showed little vertical differences, with values of approximately 1 FTU from the surface down to 55 m depth, and a gradual increase to a value of 3 FTU at the bottom (70 m depth).

The water samples collected at the beginning and end of the instrument deployment were extremely clear. For all 5 replicates performed on each sample, TSS was essentially undetectable (below 0.1 $mg \cdot l^{-1}$). Thus, results are not reported here.

4.0 DISCUSSION

4.1 Sediment Resuspension by Bottom Currents

A review of the velocity profile data (Figure 3-2) showed that currents were strongest at mid-depth, reaching a maximum of approximately 45 $cm \cdot s^{-1}$, while the strongest velocities measured at 1 m above the bottom were only 26 $cm \cdot s^{-1}$. Data on near-bottom turbidity collected by an optical backscatter sensor (OBS) showed that local resuspension of bottom sediments by tidal currents is unlikely, as the relatively few peaks in turbidity were associated with any increases in near-bottom current velocity. A hydrocast with a CTD equipped with an OBS sensor showed that background turbidity in the water column was also extremely low, (below 4 FTU). A TSS analysis on a water sample collected near-bottom confirmed this observation showing undetectable amounts of suspended solids. Thus, during the August 2001 deployment period, water column turbidity at the Rockland Disposal Site was very low. Given that the deployment period did not include the passage of any major weather systems, this study cannot make any conclusive statements about the potential for sediment resuspension during major ocean storms.

4.2 Mean Current Profiles

For the purposes of future disposal plume modeling, velocity data from only five depth levels are required. Nevertheless, it is of interest to examine more detailed profiles, given the capability of the ADCP. Long-term mean profiles and histograms of current direction illustrate the differences between near-surface, mid-depth, and near-bottom currents in the late summer. Mean vector magnitude was low throughout the water column (approximately 3 $cm \cdot s^{-1}$) and some shear existed in the profile, with higher magnitudes at mid to lower depths (40 to 60 m); in fact, some near-surface magnitude values were lower than those near bottom. Mean current direction, which was northward at the near surface rotating to easterly at near-bottom, demonstrated that the average long-term current direction was not necessarily aligned with the tidal flows.

The profile of mean speed indicated near-surface values appeared to be approaching 15 $cm \cdot s^{-1}$ at a depth of 9 m with a gradual reduction in speed to a depth of 30 m. Mean current speed increased to 15 $cm \cdot s^{-1}$ between 30 m and 40 m depth, with higher values (> 15 $cm \cdot s^{-1}$) in the middle to lower water column (40 to 60 m depth). A decrease in mean speed (16 $cm \cdot s^{-1}$ to 9 $cm \cdot s^{-1}$) primarily attributed to the effects of local bathymetry and bottom friction was identified between 60 to 69 m depth. Thus, when compared to the results of the tidal analysis, the mean current speed profile for the water column demonstrated that shear in flow over RDS can be directly attributed to tidal currents.

4.3 Tidal Currents and Residual Flow

The most significant finding from the tidal analysis was that the currents were more tidal in nature than anticipated. At some depth levels, currents were more than 95% tidal, based on variance calculations. As is typical in this region, the M_2, N_2, S_2, and L_2 constituents were the most significant. Given the overall trend of currents in time (with increasing maximum velocities in the middle of the record), a significant fortnightly or monthly component was expected. However, the harmonic analysis had difficulty separating these constituents with confidence, as was evident in the error calculated (Tables 3-4 and 3-5).

The eccentricity of tidal ellipses was in agreement with currents in a channel, with little to no minor axis, and the inclination of the major axis aligned with the channel axis. The somewhat different inclination of the near-bottom ellipse may be associated with local bathymetry.

Residual flow during the deployment period was quite low. In comparing the structure of near-surface residual currents and wind patterns, it was obvious that winds were the most important factor in driving sub-tidal flow in the near-surface layers. Interestingly, both mean currents (Figure 3-5) and residual currents (Figure 3-7) appeared to be rotated somewhat counterclockwise from the wind direction for a given event, as from 16 to 19 August. The usefulness of tide-subtracted residual flow was evident in this type of comparison. Mean flow vectors showed this event to have the strongest residual velocities, even though the corresponding wind event was not the most significant in the wind record. This wind event did exhibit the most sustained wind velocities in a given direction, and thus the water column response showed higher mean velocities for this period. The strongest event in the residual flow calculation (at a value of approximately 22 $cm \cdot s^{-1}$ on 4 September) did correspond to the period of highest wind velocities (approximately 8 $m \cdot s^{-1}$).

4.4 Progressive Vector Diagrams for Plume Drift Predictions

In an effort to better understand the potential for the transport of material in the water column associated with disposal activity, progressive vector diagrams (PVDs) were plotted for different periods and depth levels. The PVDs represent a cumulative vector of the current data collected at the point location. They do not necessarily represent the actual path of entrained sediment particles, as is it is not possible to extrapolate in space the effects of currents that were observed at a single point. Nevertheless, they are useful in obtaining a first-order comparison of currents at different depth levels. The time extent of the diagrams was restricted to periods on the order of typical plume suspension time frames.

Two timescales were chosen for this presentation: one-hour and three-hour diagrams. Suspended sediment plumes from dredging disposal operations have been shown to persist for varying durations. The first goal in plotting the PVDs was to determine at what timescale a water parcel trajectory would remain approximately within the confines of the disposal site. Having shown this, it was then decided to expand this timescale several times. In Figure 4-1, the 1-hour PVDs were plotted for both an ebb tide (dashed) and a flood tide (solid). The data were chosen from the middle of the dataset with the strongest tidal currents, starting at slack tide for each case. After one hour, current vectors tended to stay within the disposal site boundaries at all depth levels. Excursions were greater for the ebb tide than flood tide. Near surface current vectors extended outward for approximately 0.5 kilometers beyond the boundaries. The alignment of the diagrams with the computed tidal axes agrees well for the near-surface and near-bottom, but not as well for the mid-depth level. In this particular instance, the mid-depth currents trend more northwest-southeast than the other depth levels.

In Figure 4-2, the PVDs for both ebb (dashed) and flood (solid) tidal cycles were plotted for a 3-hour period. Excursions were greatest in the lower water column, extending approximately 2.25 km from the origin. This was not surprising, given the structure of mean speed profiles. Excursions were higher for the flood tide than the ebb tide at all depth levels. Surface current vectors turned slightly, and were therefore most likely not in phase with the other depth levels. Two progressive vector diagrams showed that for the most part, excursions were in the same direction for each depth level, even though they were derived from different portions of the dataset. This reinforces the fact that currents are primarily tidal, and thus quite consistent and predictable.

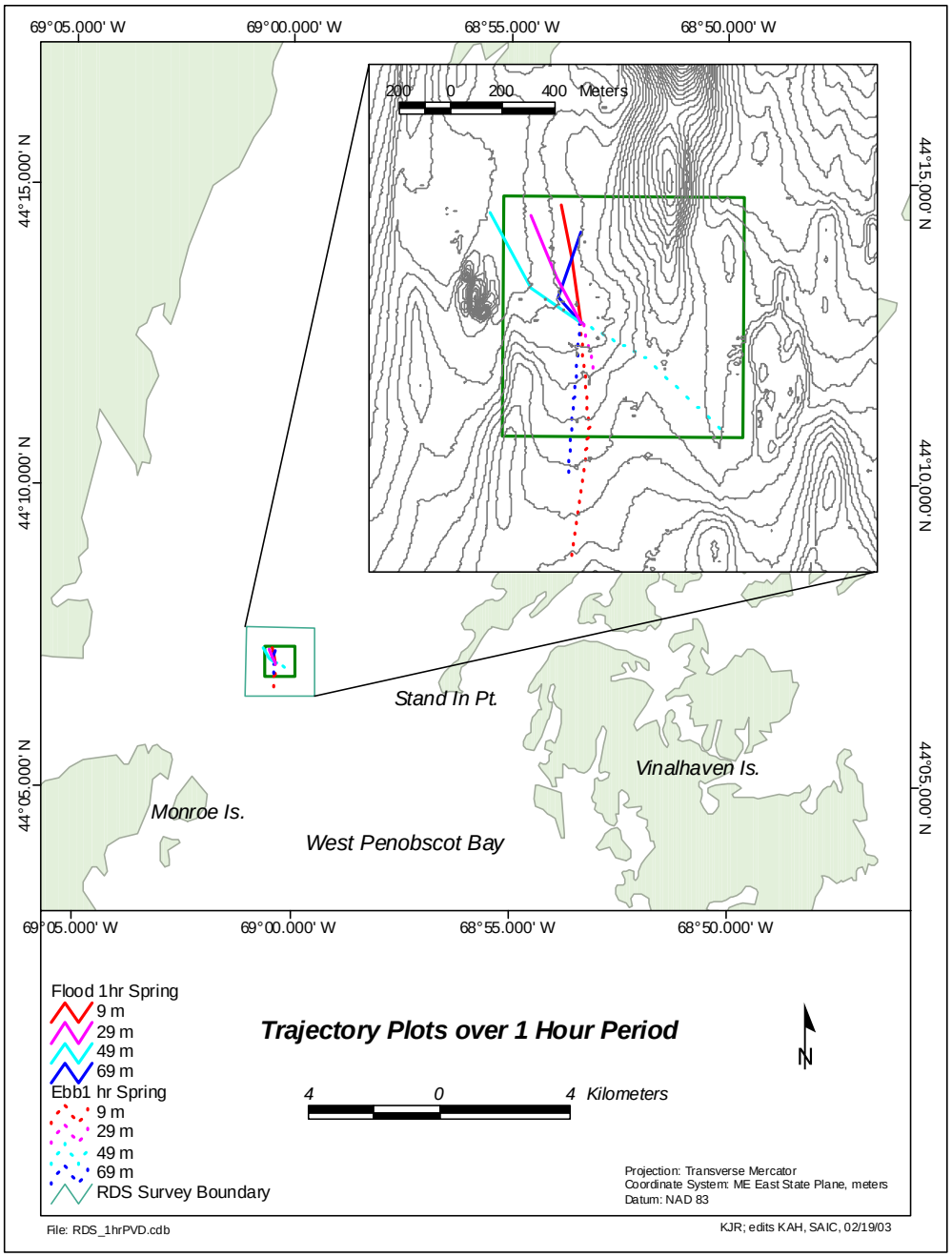

Figure 4-1. One-hour progressive vector diagrams from spring portion of tide cycle at ADCP depth levels 9 m (red), 49 m (cyan) and the Aquadopp at 69 m (blue) for flood cycle (solid lines) and ebb cycle (dashed lines).

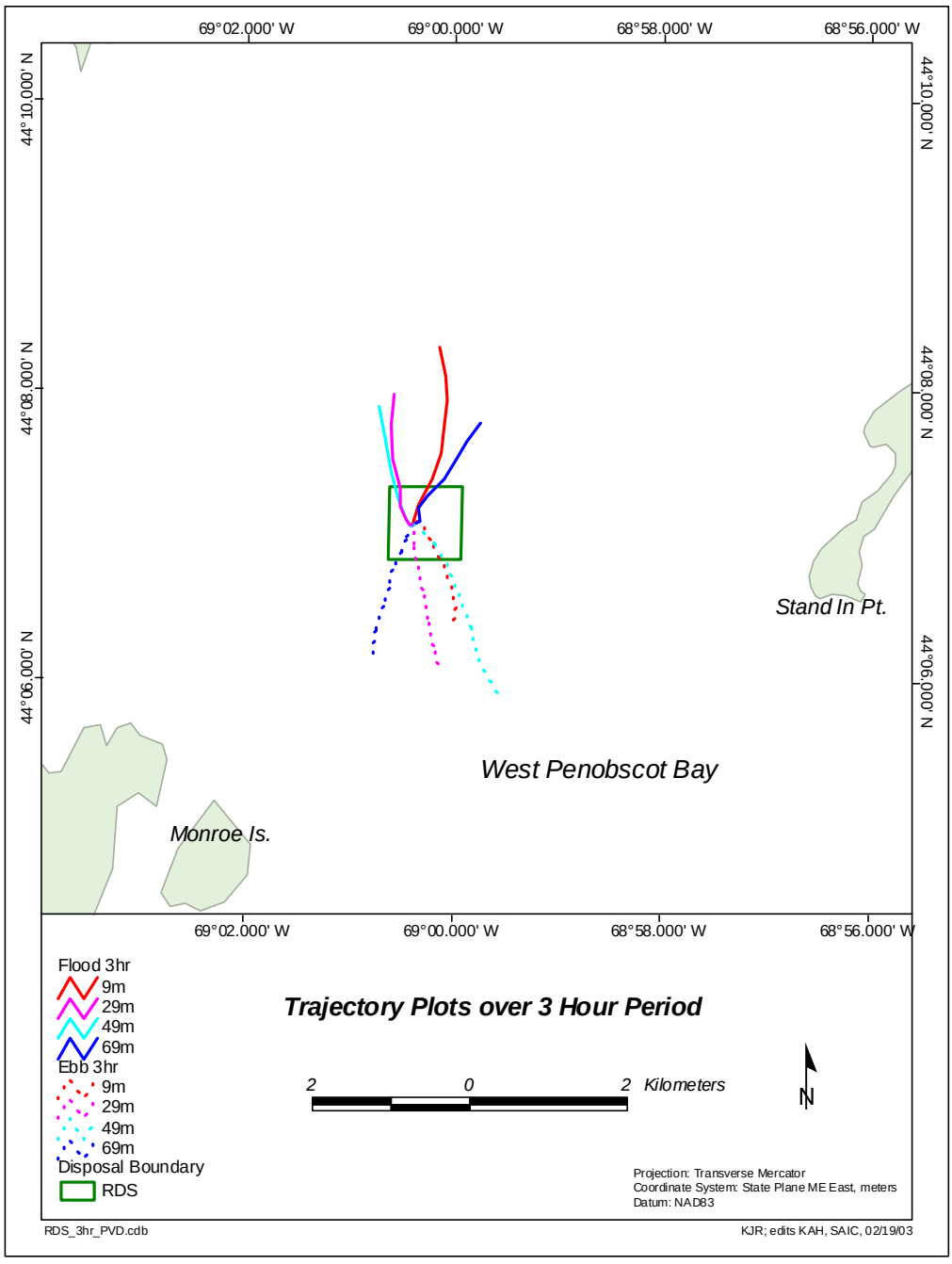

Figure 4-2. Three-hour progressive vector diagrams from ADCP depth levels 9 m (red), 49 m (cyan), and the Aquadopp at 69 m (blue) for flood cycle (solid lines) and ebb cycle (dashed lines).

5.0 CONCLUSIONS

A one-month deployment of current meters and turbidity sensors at the Rockland Disposal Site revealed important information on the vertical and temporal variability of water column currents at the site. Vector mean magnitude averaged over the entire record showed weak mean flow on the order of 3 $cm \cdot s^{-1}$, with somewhat stronger currents at lower depth levels (45 to 55 m depth). Vector mean direction was to the north at the surface, rotating clockwise to the east near the bottom. Mean speed, calculated independent of direction, showed higher velocities in the mid to lower water column, in agreement with tidal observations. Histograms of directional data confirm the bi-directional nature of the currents.

Maximum velocities of approximately 45 $cm \cdot s^{-1}$ were detected in the mid-water column, centered at 49 m depth, while maximum near bottom velocities were only 26 $cm \cdot s^{-1}$. Turbidity data showed that resuspension of local sediments due to tidal currents is unlikely at this site, as there were no significant turbidity events, and the near-bottom currents were weak. No significant storm events occurred during the August 2001 deployment period. Thus, the potential effects of storms on resuspension of fine-grained sediments could not be ascertained by this study. However, given the deep nature of the site and its relatively protected position, it is unlikely that storm generated waves would be felt at the bottom at RDS, due to the attenuation of wave-induced orbital currents with depth.

As anticipated, the semidiurnal tide was the most significant feature in the velocity record at all depths, with a pronounced bi-directional nature. Spring-neap modulation of the semidiurnal tide was clearly evident at all depths, but most obvious in mid-water column velocities. A full harmonic analysis confirmed the M_2 lunar tide component was most significant, with the N_2 and S_2 representing the next largest constituents. Tidal phase comparisons between depth levels indicated that for the major tidal constituents, the surface and bottom currents were slightly ahead of the mid-water column.

The effects of other low frequency processes were notable in a low-pass filtered plot of currents, where flows superimposed on the tidal signal were noted. More specifically, near surface residual flow mimicked the wind patterns quite well, and evidence existed for deep water column response to such near-surface wind driven events. Residual currents were calculated by subtracting the harmonic tidal fit from the raw data and provided an accurate measure of the water column response to wind events. Residual near-bottom currents were weak (typically 5 $cm \cdot s^{-1}$ or less), and exhibited an easterly flow during the

study period. No major weather systems were encountered during the 32-day deployment, and residual currents remained generally weak throughout the entire water column.

Construction of progressive vector diagrams (PVDs) was performed for typical timeframes of dredged material settlement (1 hour or less). These indicated that most cumulative current vectors remained within the confines of the disposal site at all depth levels after one hour. When plotting PVDs for a 3 hour period, maximum excursions from the current meter location of approximately 2.25 km were noted at the near-surface levels, and approximately 1.25 km at near-bottom levels.

6.0 REFERENCES

Foreman, M.G.G. "Manual for tidal heights analysis and prediction." Pacific Marine Science Report 77-10 (1977)

GoMOOS, Gulf of Maine Ocean Observing System, University of Maine Physical Oceanography Group, http://gyre.umeoce.maine.edu/index.html, September 2001.

Morris, J. T. 1996. DAMOS Site Management Plan, April 1996. SAIC Report No. 365, US Army Corps of Engineers, New England District, Concord, MA.

NCASI Technical Bulletin No. 291, March 1977. National Council of the Paper Industry for Air and Stream Improvement, Inc., 260 Madison Avenue, New York, NY.

SAIC. 2001. Monitoring Cruise at the Rockland Disposal Site, September 2000. DAMOS Contribution No. 131, SAIC Report No. 350, US Army Corps of Engineers, New England District, Concord, MA.

APPENDIX A

Appendix A
Disposal Log Summary
1990—2001

1990 RDS

Project: CASTRAL HARBOR
Permit Number: 198803537 **Permittee:** MAINE MARITIME ACADEMY

Project Total Volume: 421 CM 550 CY

Project: ROCKLAND HARBOR
Permit Number: 198800818 **Permittee:** FJ OHARA

Project Total Volume: 2,122 CM 2,775 CY

Project: WAYFARER MARINA
Permit Number: 198803544 **Permittee:** WAYFARER MARINE CORP.

Project Total Volume: 6,920 CM 9,050 CY

1991 RDS

Project: CAMDEN YACHT CLUB
Permit Number: 198801262 **Permittee:** TOWN OF CAMDEN

Project Total Volume: 237 CM 310 CY

Project: FISHERMANS WHARF
Permit Number: 198801573 **Permittee:** CITY OF ROCKLAND

Project Total Volume: 115 CM 150 CY

Project: CASTRAL HARBOR
Permit Number: 198803537 **Permittee:** MAINE MARITIME ACADEMY

Project Total Volume: 191 CM 250 CY

1991 RDS (continued)

Project: CAMDEN HARBOR

Permit Number: 198900799 **Permittee:** TOWN OF CAMDEN

Project Total Volume: 3,131 CM 4,095 CY

1992 RDS

Project: SEARS HBR

Permit Number: 199100322 **Permittee:** TOWN OF SEARSPORT

Project Total Volume: 2,374 CM 3,105 CY

1993 RDS

Project: CAMDEN YACHT CLUB

Permit Number: 198801262 **Permittee:** TOWN OF CAMDEN

Project Total Volume: 130 CM 170 CY

Project: CAMDEN HARBOR

Permit Number: 198900799 **Permittee:** TOWN OF CAMDEN

Project Total Volume: 1,552 CM 2,030 CY

Project: ROCKLAND HARBOR

Permit Number: 199300313 **Permittee:** NORTHEND SHIPYARD INC

Project Total Volume: 554 CM 725 CY

Project: BANGOR & AROOSTOCK PIER

Permit Number: 199300809 **Permittee:** BANGOR AND AROOSTOCK RAILWAY C

Project Total Volume: 2,347 CM 3,070 CY

1994 RDS

Project: BANGOR & AROOSTOCK PIER

Permit Number: 199300809 **Permittee:** BANGOR AND AROOSTOCK RAILWAY C

Project Total Volume: 382 CM 500 CY

Project: MUNICIPAL FISH PIER

Permit Number: 199401060 **Permittee:** CITY OF ROCKLAND

Project Total Volume: 1,335 CM 1,745 CY

1995 RDS

Project: PORTLAND HARBOR

Permit Number: 199403124 **Permittee:** PROPRIETORS OF UNION WHARF

Project Total Volume: 398 CM 520 CY

1999 RDS

Project: TRAVEL LIFT

Permit Number: 199802804 **Permittee:** WAYFARER MARINE CORP.

Project Total Volume: 2,225 CM 2,910 CY

2000 RDS

Project: TRAVEL LIFT

Permit Number: 199802804 **Permittee:** WAYFARER MARINE CORP.

Project Total Volume: 77 CM 100 CY

Project: CAMDEN HARBOR

Permit Number: 199901904 **Permittee:** WAYFARER MARINE CORP.

Project Total Volume: 1,850 CM 2,420 CY

Report Total Volume: 26,360 CM 34,475 CY
1990-2000

2001 RDS

Project: ROCKLAND HARBOR

Permit: 200001733 **Permittee:** ATLANTIC CHALLENGE

Project Total Volume: 10,353 CM 13,540 CY

Report Total Volume: 10,353 CM 13,540 CY
2001

APPENDIX B

Appendix B-1. Ellipse Parameters for L_2 Tidal Constituent (Period of 12.2 Hours - Major and Minor Axis Values in $cm \cdot s^{-1}$, Inclination and Phase in Degrees)

Depth	Major	Error	Minor	Error	Inclination	Error	Phase	Error
9 m	1.98	0.96	0.27	0.87	124.46	25.69	90.72	28.32
19 m	1.46	0.74	0.27	0.58	152.91	24.11	121.95	30.14
29 m	1.20	0.64	0.23	0.64	44.72	31.95	15.54	32.04
39 m	1.94	0.59	-0.74	0.46	80.38	17.49	58.53	21.06
49 m	2.22	0.54	-0.90	0.68	111.25	21.81	64.32	18.57
59 m	2.58	0.48	-0.64	0.62	93.20	14.89	45.79	11.85
69 m	1.54	0.39	-0.31	0.33	36.82	13.15	48.11	15.21

Appendix B-2. Ellipse Parameters for M_4 Tidal Constituent (Period of 6.21 Hours - Major and Minor Axis Values in $cm \cdot s^{-1}$, Inclination and Phase in Degrees)

Depth	Major	Error	Minor	Error	Inclination	Error	Phase	Error
9 m	2.45	0.57	-1.04	0.62	117.66	18.91	113.27	17.91
19 m	0.72	0.61	-0.52	0.33	3.14	94.08	302.87	111.42
29 m	0.90	0.42	-0.47	0.53	61.49	50.37	5.92	44.21
39 m	0.54	0.54	-0.24	0.47	102.89	69.46	23.22	75.92
49 m	1.47	0.39	-0.29	0.26	71.35	10.75	3.96	15.77
59 m	1.54	0.51	-0.26	0.41	67.80	15.88	356.62	19.37
69 m	1.09	0.37	-0.55	0.31	73.23	25.20	349.59	27.79

Appendix B-3. Ellipse Parameters for K_1 Tidal Constituent (Period of 23.92 Hours - Major and Minor Axis Values in $cm \cdot s^{-1}$, Inclination and Phase in Degrees)

Depth	Major	Error	Minor	Error	Inclination	Error	Phase	Error
9 m	0.95	0.07	0.08	0.05	66.78	3.30	46.22	4.33
19 m	0.76	0.30	0.37	0.34	174.94	36.56	191.70	33.85
29 m	0.81	0.13	0.09	0.19	84.55	13.43	114.41	9.61
39 m	1.05	0.22	0.60	0.22	100.11	20.28	133.63	20.38
49 m	0.99	0.07	0.28	0.20	95.51	12.21	137.06	5.56
59 m	1.49	0.25	0.13	0.17	86.25	6.41	126.77	9.67
69 m	0.95	0.07	0.08	0.05	66.78	3.30	106.38	4.33

Appendix B-4. Ellipse Parameters for O_1 Tidal Constituent (Period of 25.84 Hours - Major and Minor Axis Values in $cm \cdot s^{-1}$, Inclination and Phase in Degrees)

Depth	Major	Error	Minor	Error	Inclination	Error	Phase	Error
9 m	0.70	0.07	0.17	0.06	58.91	5.19	25.97	6.11
19 m	0.20	0.31	-0.11	0.33	28.33	144.72	201.32	139.19
29 m	0.45	0.17	-0.23	0.15	146.42	29.79	64.17	32.19
39 m	0.97	0.22	-0.10	0.22	89.67	12.93	80.94	13.06
49 m	0.68	0.08	-0.01	0.19	104.13	15.99	80.30	6.81
59 m	0.89	0.25	0.12	0.17	100.81	11.13	82.97	16.16
69 m	0.70	0.07	0.17	0.06	58.91	5.19	81.74	6.11

Appendix B-5. Ellipse Parameters for M_{sf} Tidal Constituent (Period of 357.14 Hours or 14.88 Days – also known as Semi-Fortnightly - Major and Minor Axis Values in $cm \cdot s^{-1}$, Inclination and Phase in Degrees)

Depth	Major	Error	Minor	Error	Inclination	Error	Phase	Error
9 m	2.13	4.14	0.10	0.81	98.28	22.36	318.49	111.68
19 m	1.70	0.28	0.19	0.50	64.50	17.06	116.23	9.75
29 m	1.47	1.60	0.49	1.11	60.63	54.29	147.03	72.34
39 m	1.00	1.93	0.40	1.21	61.65	97.56	142.23	135.32
49 m	0.68	0.94	0.47	0.80	5.40	168.53	128.66	178.62
59 m	1.44	0.89	0.34	0.41	80.83	19.39	242.03	37.68
69 m	1.29	0.98	0.17	0.75	61.49	34.34	240.50	44.51

Appendix B-6. Ellipse Parameters for M_f Tidal Constituent (Period of 666.67 Hours or 27.78 Days - Major and Minor Axis Values in $cm \cdot s^{-1}$, Inclination and Phase in Degrees)

Depth	Major	Error	Minor	Error	Inclination	Error	Phase	Error
9 m	0.70	0.07	0.17	0.06	58.91	5.19	25.97	6.11
19 m	0.20	0.31	-0.11	0.33	28.33	144.72	201.32	139.19
29 m	0.45	0.17	-0.23	0.15	146.42	29.79	64.17	32.19
39 m	0.97	0.22	-0.10	0.22	89.67	12.93	80.94	13.06
49 m	0.68	0.08	-0.01	0.19	104.13	15.99	80.30	6.81
59 m	0.89	0.25	0.12	0.17	100.81	11.13	82.97	16.16
69 m	0.70	0.07	0.17	0.06	58.91	5.19	81.74	6.11

INDEX